

WESTINGHOUSE CLASS 3
CUSTOMER DESIGNATED DISTRIBUTION

WCAP-10509

ANALYSIS OF CAPSULE T FROM THE
TENNESSEE VALLEY AUTHORITY
SEQUOYAH UNIT 2 REACTOR VESSEL
RADIATION SURVEILLANCE PROGRAM

R. S. Boggs
S. E. Yanichko
C. A. Cheney
W. T. Kaiser

April 1984

Work performed under Shop Order No. UEN-6620

APPROVED: 

T. R. Mager, Manager
Metallurgical and NDE Analysis

Prepared by Westinghouse for the Tennessee Valley Authority

Although information contained in this report is nonproprietary, no distribution shall be made outside Westinghouse or its licensees without the customer's approval.

WESTINGHOUSE ELECTRIC CORPORATION
Nuclear Energy Systems
P.O. Box 355
Pittsburgh, Pennsylvania 15230

8408060231 840731
PDR ADOCK 05000328
P PDR

PREFACE

This report has been technically reviewed and verified.

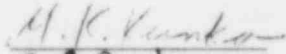
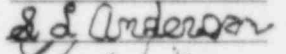
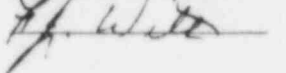
	<i>Reviewer</i>
Sections 1 through 5 and 7	M. K. Kunka 
Section 6	S. L. Anderson 
Appendix A	F. J. Witt 

TABLE OF CONTENTS

Section	Title	Page
1	SUMMARY OF RESULTS	1-1
2	INTRODUCTION	2-1
3	BACKGROUND	3-1
4	DESCRIPTION OF PROGRAM	4-1
5	TESTING OF SPECIMENS FROM CAPSULE T	5-1
	5-1. Overview	5-1
	5-2. Charpy V-Notch Impact Test Results	5-3
	5-3. Tension Test Results	5-3
	5-4. Wedge Opening Loading Tests	5-4
6	RADIATION ANALYSIS AND NEUTRON DOSIMETRY	6-1
	6-1. Introduction	6-1
	6-2. Discrete Ordinates Analysis	6-1
	6-3. Neutron Dosimetry	6-6
	6-4. Transport Analysis Results	6-11
	6-5. Dosimetry Results	6-21
7	SURVEILLANCE CAPSULE REMOVAL SCHEDULE	7-1
8	REFERENCES	8-1

TABLE OF CONTENTS (cont)

Section	Title	Page
Appendix A	HEATUP AND COOLDOWN LIMIT CURVES FOR NORMAL OPERATION	A-1
	A-1. Introduction	A-1
	A-2. Fracture-Toughness Properties	A-1
	A-3. Criteria For Allowable Pressure-Temperature Relationships	A-5
	A-4. Heatup and Cooldown Limit Curves	A-7

LIST OF ILLUSTRATIONS

Figure	Title	Page
4-1	Arrangement of Surveillance Capsules in the Sequoyah Unit 2 Reactor Vessel (Updated Lead Factors for Capsules Shown in Parentheses)	4-3
4-2	Capsule T Diagram Showing Location of Specimens, Thermal Monitors, and Dosimeters	4-5
5-1	Irradiated Charpy V-Notch Impact Properties for Sequoyah Unit 2 Reactor Vessel Intermediate Shell Forging 05 (Axial Orientation)	5-15
5-2	Irradiated Charpy V-Notch Impact Properties for Sequoyah Unit 2 Reactor Vessel Intermediate Shell Forging 05 (Tangential Orientation)	5-16
5-3	Irradiated Charpy V-Notch Impact Properties for Sequoyah Unit 2 Reactor Pressure Vessel Weld Metal	5-17
5-4	Irradiated Charpy V-Notch Impact Properties for Sequoyah Unit 2 Reactor Pressure Vessel Weld Heat Affected Zone Metal	5-18
5-5	Charpy Impact Specimen Fracture Surfaces for Sequoyah Unit 2 Pressure Vessel Intermediate Shell Forging 05 (Axial Orientation)	5-19
5-6	Charpy Impact Specimen Fracture Surfaces for Sequoyah Unit 2 Pressure Vessel Intermediate Shell Forging 05 (Tangential Orientation)	5-20
5-7	Charpy Impact Specimen Fracture Surfaces for Sequoyah Unit 2 Weld Metal	5-21
5-8	Charpy Impact Specimen Fracture Surfaces for Sequoyah Unit 2 Weld Heat Affected Zone Metal	5-22

LIST OF ILLUSTRATIONS (cont)

Figure	Title	Page
5-9	Comparison of Actual versus Predicted 30 ft lb Transition Temperature Increases for the Sequoyah Unit 2 Reactor Vessel Material based on the Prediction Methods of Regulatory Guide 1.99 Revision 1	5-23
5-10	Tensile Properties for Sequoyah Unit 2 Reactor Vessel Intermediate Shell Forging 05 (Axial Orientation)	5-24
5-11	Tensile Properties for Sequoyah Unit 2 Reactor Vessel Weld Metal	5-25
5-12	Fractured Tensile Specimens of Sequoyah Unit 2 Reactor Vessel Intermediate Shell Forging 05 (Axial Orientation) and Weld Metal	5-26
5-13	Typical Stress-Strain Curve for Tension Specimens	5-27
6-1	Sequoyah Unit 2 Reactor Geometry	6-2
6-2	Plan View of a Reactor Vessel Surveillance Capsule	6-4
6-3	Calculated Azimuthal Distribution of Maximum Fast-Neutron Flux ($E > 1.0$ MeV) within the Pressure Vessel Surveillance Capsule Geometry	6-12
6-4	Calculated Radial Distribution of Maximum Fast-Neutron Flux ($E > 1.0$ MeV) within the Pressure Vessel	6-13
6-5	Relative Axial Variation of Fast-Neutron Flux ($E > 1.0$ MeV) within the Pressure Vessel	6-14
6-6	Calculated Radial Distribution of Fast-Neutron Flux ($E > 1.0$ MeV) within the Reactor Vessel Surveillance Capsules	6-15

LIST OF ILLUSTRATIONS (cont)

Figure	Title	Page
6-7	Calculated Variation of Fast-Neutron Flux Monitor Saturated Activity within Capsules Located at 40 Degrees	6-16
6-8	Calculated Variation of Fast-Neutron Flux Monitor Saturated Activity within Capsules Located at 4 Degrees	6-17
A-1	Predicted Adjustment of Reference Temperature, ΔRT_{NDT} as a Function of Fluence and Copper Content	A-2
A-2	Fast Neutron Fluence ($E > 1.0$ MeV) as a Function of Full Power Service Life	A-3
A-3	Sequoyah Unit 2 Reactor Coolant System Heatup Limitations Applicable up to 9 EFPY	A-8
A-4	Sequoyah Unit 2 Reactor Coolant System Cooldown Limitations Applicable up to 9 EFPY	A-9

LIST OF TABLES

Table	Title	Page
4-1	Chemical Composition and Heat Treatment of the Sequoyah Unit 2 Reactor Vessel Surveillance Materials	4-4
5-1	Charpy V-Notch Impact Data for the Sequoyah Unit 2 Intermediate Shell Forging 05 (Axial Orientation) Irradiated at 550°F, Fluence 2.20×10^{18} n/cm ² (E > 1 MeV)	5-5
5-2	Charpy V-Notch Impact Data for the Sequoyah Unit 2 Intermediate Shell Forging 05 (Tangential Orientation) Irradiated at 550°F, Fluence 2.20×10^{18} (E > 1 MeV)	5-6
5-3	Charpy V-Notch Impact Data for the Sequoyah Unit 2 Pressure Vessel Weld Metal irradiated at 550°F, Fluence 2.20×10^{18} n/cm ² (E > 1 MeV)	5-7
5-4	Charpy V-Notch Impact Data for the Sequoyah Unit 2 Pressure Vessel Weld Heat Affected Zone Metal Irradiated at 550°F, Fluence 2.20×10^{18} (E > 1 MeV)	5-8
5-5	Instrumented Charpy Impact Test Results for Sequoyah Unit 2 Intermediate Shell Forging 05 (Axial Orientation)	5-9
5-6	Instrumented Charpy Impact Test Results for the Sequoyah Unit 2 Intermediate Shell Forging 05 (Tangential Orientation)	5-10
5-7	Instrumented Charpy Impact Test Results for Sequoyah Unit 2 Weld Metal	5-11
5-8	Instrumented Charpy Impact Test Results for Sequoyah Unit 2 Heat Affected Zone Metal	5-12
5-9	The Effect of 550°F Irradiation at 2.20×10^{18} (E > 1 MeV) on the Notch Toughness Properties of the Sequoyah Unit 2 Reactor Vessel Materials	5-13

LIST OF TABLES (cont.)

Table	Title	Page
5-10	Tensile Properties for Sequoyah Unit 2 Reactor Vessel Material Irradiated to 2.20×10^{18} n/cm ²	5-14
6-1	47 Group Energy Structure	6-5
6-2	Nuclear Constants for Neutron Flux Monitors Contained in the Sequoyah Unit 2 Surveillance Capsules	6-7
6-3	Calculated Fast-Neutron Flux ($E > 1.0$ MeV) and Lead Factors for Sequoyah Unit 2 Surveillance Capsules	6-18
6-4	Calculated Neutron Energy Spectra at the Center of Sequoyah Unit 2 Surveillance Capsules	6-19
6-5	Spectrum-Averaged Reaction Cross Sections at the Center of Sequoyah Unit 2 Surveillance Capsules	6-20
6-6	Irradiation History of Sequoyah Unit 2 Reactor Vessel Surveillance Capsule T	6-22
6-7	Comparison of Measured and Calculated Fast-Neutron Flux Monitor Saturated Activities for Capsule T	6-23
6-8	Results of Fast-Neutron Dosimetry for Capsule T	6-24
6-9	Results of Thermal-Neutron Dosimetry for Capsule T	6-25
6-10	Summary of Neutron Dosimetry Results for Capsule T	6-25
A-1	Sequoyah Unit 2 Reactor Vessel Toughness Data	A-4

SECTION 1

SUMMARY OF RESULTS

The analysis of the reactor vessel material contained in Capsule T, the first surveillance capsule to be removed from the Tennessee Valley Authority Sequoyah Unit 2 reactor pressure vessel, led to the following conclusions:

- Irradiation of the reactor vessel intermediate shell forging 05, to 2.20×10^{18} n/cm, resulted in both 30 and 50 ft-lb transition temperature increases of 25°F for specimens oriented normal to the major working direction (axial orientation) and 60°F for specimens oriented in the major working direction (tangential orientation).
- Weld metal irradiated to 2.20×10^{18} n/cm² resulted in a 30 and 50 ft-lb transition temperature increase of 80 and 75°F, respectively.
- The average upper shelf energy of the limiting forging (05) decreased from 88 to 82 ft-lbs and the limiting weld metal decreased from 112 to 110 ft-lbs. Both materials exhibit a more than adequate shelf level for continued safe plant operation.
- Comparison of the 30 ft-lb transition temperature increases for the Sequoyah Unit 2 surveillance material with predicted increases using the methods of NRC Regulatory Guide 1.99, Revision 1, shows that the weld metal transition temperature increase was greater than predicted. Since the transition temperature increase was greater than predicted, the future operating limits for the vessel, shown in Appendix A, were based on a predicted trend curve which passed through the actual increase in transition temperature as determined from the irradiated weld metal specimens.

SECTION 2 INTRODUCTION

This report presents the results of the examination of Capsule T, the first capsule to be removed from the reactor in the continuing surveillance program which monitors the effects of neutron irradiation on Sequoyah Unit 2 reactor pressure vessel materials under actual operating conditions.

The surveillance program for Sequoyah Unit 2 reactor pressure vessel materials was designed and recommended by the Westinghouse Electric Corporation. A description of the surveillance program and the preirradiation mechanical properties of the reactor vessel materials are presented by Yanichko.⁽¹⁾ The surveillance program was planned to cover the 40-year design life of the reactor pressure vessel and was based on ASTM E-185-73, "Recommended Practice for Surveillance Tests for Nuclear Reactors."⁽²⁾ Westinghouse Nuclear Energy Systems personnel were contracted for the preparation of procedures for removing the capsule from the reactor and its shipment to the Westinghouse Research and Development Laboratory, where the postirradiation mechanical testing of the Charpy V-notch impact and tensile surveillance specimens was performed.

This report summarizes testing and the postirradiation data obtained from surveillance Capsule T removed from Sequoyah Unit 2 reactor vessel, and discusses the analysis of these data.

SECTION 3 BACKGROUND

The ability of the large steel pressure vessel containing the reactor core and its primary coolant to resist fracture constitutes an important factor in ensuring safety in the nuclear industry. The beltline region of the reactor pressure vessel is the most critical region of the vessel because it is subjected to significant fast neutron bombardment. The overall effects of fast neutron irradiation on the mechanical properties of low alloy ferritic pressure vessel steels such as A508 Class 2 (base material of the Sequoyah Unit 2 reactor pressure vessel beltline) are well documented in the literature. Generally, low alloy ferritic materials show an increase in hardness and tensile properties and a decrease in ductility and toughness under certain conditions of irradiation.

A method for performing analyses to guard against fast fracture in reactor pressure vessels has been presented in "Protection Against Non-ductile Failure," Appendix G to Section III of the ASME Boiler and Pressure Vessel Code. The method utilizes fracture mechanics concepts and is based on the reference nil-ductility temperature RT_{NDT} .

RT_{NDT} is defined as the greater of either the drop weight nil-ductility transition temperature (NDTT per ASTM E-208) or the temperature 60°F less than the 50 ft-lb (and 35-mil lateral expansion) temperature as determined from Charpy specimens oriented normal (transverse) to the major working direction of the material. The RT_{NDT} of a given material is used to index that material to a reference stress intensity factor curve (K_{IR} curve) which appears in Appendix G of the ASME Code. The K_{IR} curve is a lower bound of dynamic, crack arrest, and static fracture toughness results obtained from several heats of pressure vessel steel. When a given material is indexed to the K_{IR} curve, allowable stress intensity factors can be obtained for this material as a function of temperature. Allowable operating limits can then be determined utilizing these allowable stress intensity factors.

RT_{NDT} and, in turn, the operating limits of nuclear power plants can be adjusted to account for the effects of radiation on the reactor vessel material properties. The radiation embrittlement or changes in mechanical properties of a given reactor pressure vessel steel can be monitored by a reactor surveillance program such as the Sequoyah Unit 2 Reactor Vessel Radiation Surveillance Program,⁽¹⁾ in which a surveillance capsule is periodically removed from the operating nuclear reactor and the encapsulated specimens

are tested. The increase in the average Charpy V-notch 30 ft-lb temperature (ΔRT_{NDT}) due to irradiation is added to the original RT_{NDT} to adjust the RT_{NDT} for radiation embrittlement. This adjusted RT_{NDT} (RT_{NDT} initial + ΔRT_{NDT}) is used to index the material to the K_{IR} curve and, in turn, to set operating limits for the nuclear power plant which take into account the effects of irradiation on the reactor vessel materials.

SECTION 4

DESCRIPTION OF PROGRAM

Eight surveillance capsules for monitoring the effects of neutron exposure on the Sequoyah Unit 2 reactor pressure vessel core region material were inserted in the reactor vessel prior to initial plant startup. The capsules were positioned in the reactor vessel between the thermal shield and the vessel wall at locations shown in Figure 4-1. The vertical center of the capsules is opposite the vertical center of the core.

Capsule T was removed after 1.04 effective full power years of plant operation. This capsule contained Charpy V-notch impact, tensile, and WOL specimens (Figure 4-2) from the intermediate shell forging 05 and submerged arc weld metal representative of the core region of the reactor vessel and Charpy V-notch specimens from weld heat-affected zone (HAZ) material.

The chemistry and heat treatment of the surveillance material are presented in Table 4-1. The chemical analyses reported in Table 4-1 were obtained from unirradiated material used in the surveillance program. In addition, a chemical analysis was performed on an irradiated Charpy specimen from the weld metal and is reported in Table 4-1.

All test specimens were machined from the 1/4 thickness location of the forgings. Test specimens represent material taken at least one forging thickness from the quenched end of the forging. Charpy specimens were machined from the forging in both the tangential (longitudinal axis of specimen parallel to the major working direction) and axial (longitudinal axis of the specimen perpendicular to the major working direction) orientations. Tensile specimens were machined from the forging with the longitudinal axis of the specimen perpendicular to the major working direction.

Charpy V-notch and tensile specimens from the weld metal were oriented with the longitudinal axis of the specimens transverse to the welding direction.

Capsule T contained dosimeter wires of pure iron, copper, nickel, and aluminum-cobalt (cadmium-shielded and unshielded). In addition, cadmium-shielded dosimeters of Neptunium (Np^{237}) and Uranium (U^{238}) were contained in the capsule and located as shown in Figure 4-2.

Thermal monitors made from two low-melting eutectic alloys and sealed in Pyrex tubes were included in the capsule and were located as shown in Figure 4-2. The two eutectic alloys and their melting points are:

2.5% Ag, 97.5% Pb

Melting Point 579°F (304°C)

1.75% Ag, 0.75% Sn, 97.5% Pb

Melting Point 590°F (310°C)

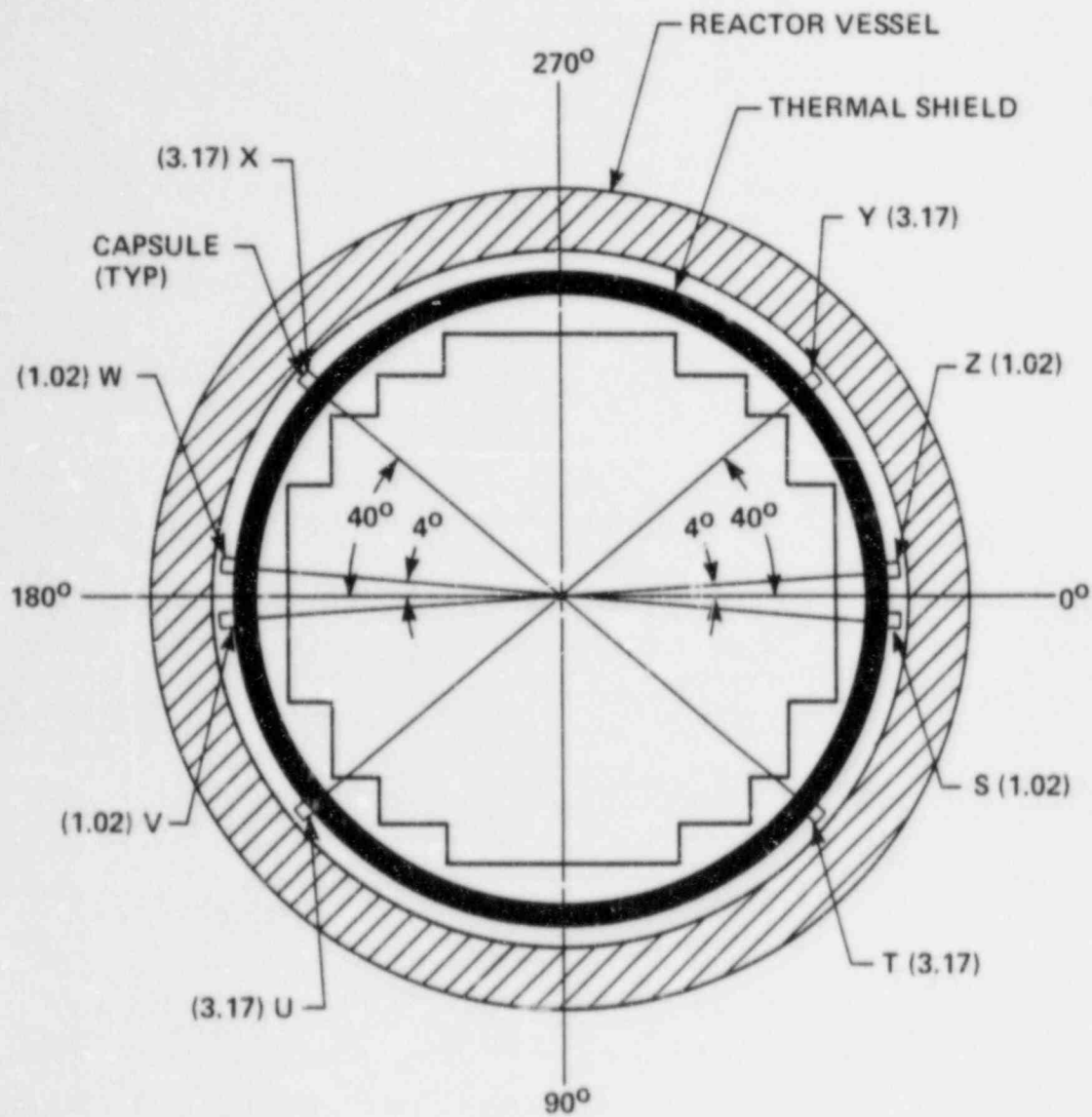


Figure 4-1. Arrangement of Surveillance Capsules in the Sequoyah Unit 2 Reactor Vessel (Updated Lead Factors for Capsules Shown in Parentheses)

TABLE 4-1

**CHEMICAL COMPOSITION AND HEAT TREATMENT OF THE
SEQUOYAH UNIT 2 REACTOR VESSEL
SURVEILLANCE MATERIALS**

Chemical Composition (WT-%)			
Element	Forging 05 Heat No. 288757/981057 Westinghouse Analysis ^(a)	Rotterdam Dockyard Analysis	Weld Metal Westinghouse Analysis ^(a)
C	0.18	0.19	0.095
S	0.018	0.013	0.013
N ₂	0.009	—	0.012
Co	0.001	—	0.001
Cu	0.13	—	0.13
Si	0.27	0.22	0.41
Mo	0.64	0.57	0.53
Ni	0.74	0.78	0.11
Mn	0.72	0.70	1.50
Cr	0.33	0.34	0.085
V	0.022	<0.01	0.002
P	0.018	0.014	0.016
Sn	0.002	—	0.002
Al	0.027	—	0.009

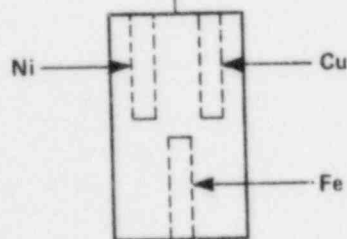
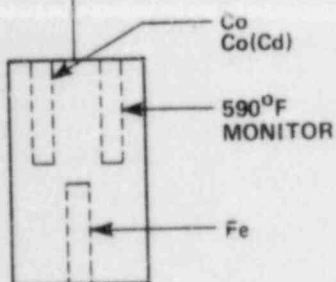
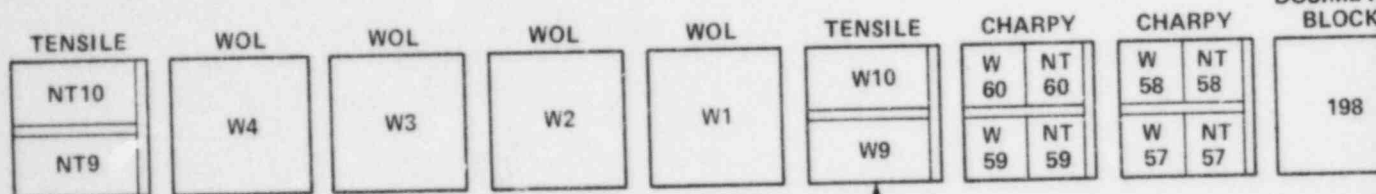
[a] All elements not listed are less than 0.010 weight%

Heat Treatment			
Material	Heat Treatment		
	Temperature (°F)	Time (hr)	Coolant
Intermediate	1675°F ± 25°F	3 1/2	Water Quenched
Shell Forging 05	1225°F ± 25°F	9	Furnace cooled to 815°F
Heat No. 288757/981057	1130°F ± 25°F	20 1/2	Furnace cooled
Weldment	1130°F ± 25°F	14 3/4	Furnace cooled

SURVEILLANCE C

Np²³⁷
U²³⁸

DOSIMET
BLOCK



← TO TOP OF VESSEL

SPECIMEN NUMBERING CODE

NT - FORGING 05 (AXIAL ORIENTATION)
NL - FORGING 05 (TANGENTIAL ORIENTATION)

W = WELD METAL
H = HEAT AFFECTED ZONE

CAPSULE T

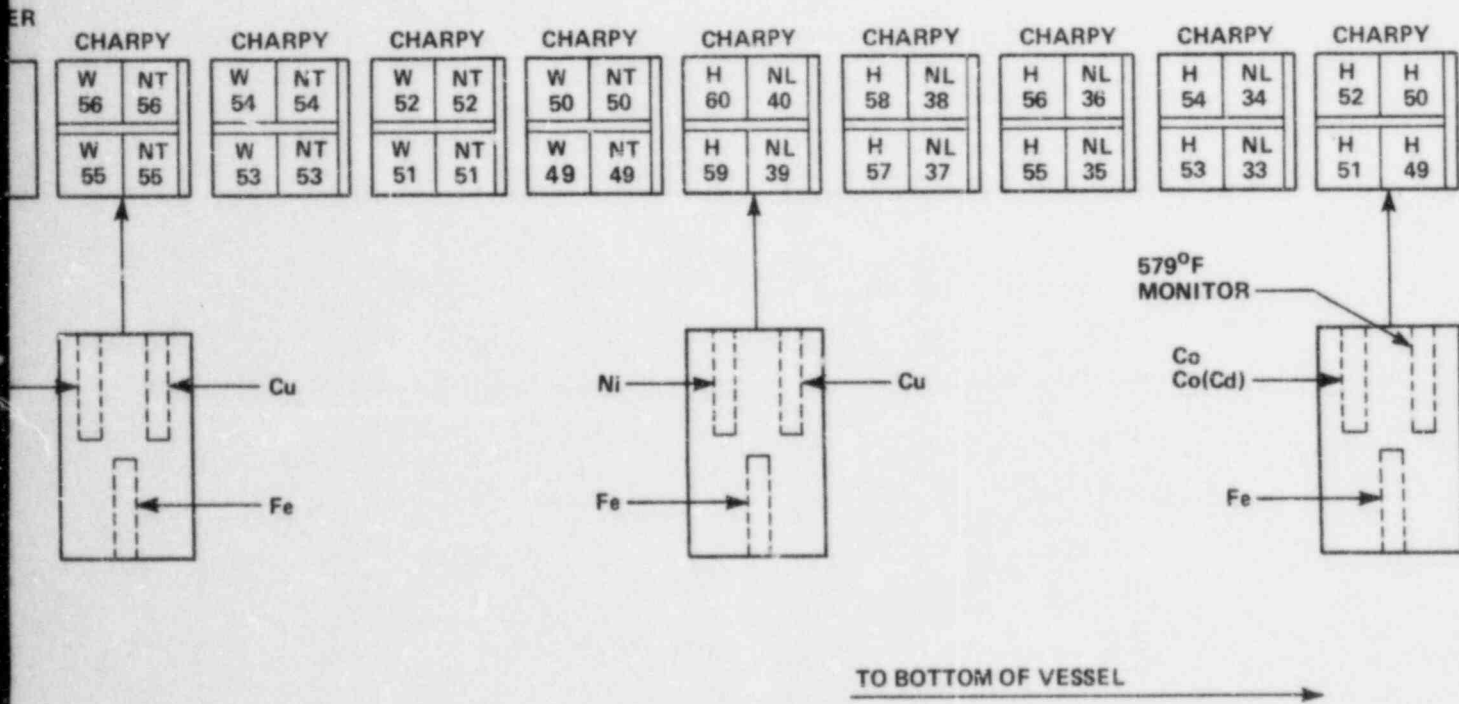


Figure 4-2. Arrangement of Specimens, Thermal Monitors, and Dosimeters in Surveillance Capsule T

SECTION 5

TESTING OF SPECIMENS FROM CAPSULE T

5-1 OVERVIEW

The postirradiation mechanical testing of the Charpy V-notch and tensile specimens was performed at the Westinghouse Research and Development Laboratory with consultation by Westinghouse Nuclear Energy Systems personnel. Testing was performed in accordance with 10CFR50, Appendices G and H, ASTM Specification E185-82 and Westinghouse Procedure MHL 7601, Revision 3 as modified by RMF Procedures 8102 and 8103.

Upon receipt of the capsule at the laboratory, the specimens and spacer blocks were carefully removed, inspected for identification number, and checked against the master list in WCAP-8513.⁽¹⁾ No discrepancies were found.

Examination of the two low-melting 304°C (579°F) and 310°C (590°F) eutectic alloys indicated no melting of either type of thermal monitor. Based on this examination, the maximum temperature to which the test specimens were exposed was less than 304°C (579°F).

The Charpy impact tests were performed per ASTM Specification E23-82 and RMF Procedure 8103 on a Tinius-Olsen Model 74, 358J machine. The tup (striker) of the Charpy machine is instrumented with an Effects Technology model 500 instrumentation system. With this system, load-time and energy-time signals can be recorded in addition to the standard measurement of Charpy energy (E_D). From the load-time curve, the load of general yielding (P_{GY}), the time to general yielding (t_{GY}), the maximum load (P_M), and the time to maximum load (t_M) can be determined. Under some test conditions, a sharp drop in load indicative of fast fracture was observed. The load at which fast fracture was initiated is identified as the fast fracture load (P_F), and the load at which fast fracture terminated is identified as the arrest load (P_A).

The energy at maximum load (E_M) was determined by comparing the energy-time record and the load-time record. The energy at maximum load is approximately equivalent to the energy required to initiate a crack in the specimen. Therefore, the propagation energy for the crack (E_p) is the difference between the total energy to fracture (E_D) and the energy at maximum load.

The yield stress (σ_y) is calculated from the three point bend formula. The flow stress is calculated from the average of the yield and maximum loads, also using the three point bend formula.

Percentage shear was determined from postfracture photographs using the ratio-of-areas methods in compliance with ASTM Specification A370-77. The lateral expansion was measured using a dial gage rig similar to that shown in the same specification.

Tension tests were performed on a 20,000-pound Instron, split-console test machine (Model 1115) per ASTM Specifications E8-81 and E21-79, and RMF Procedure 8102. All pull rods, grips, and pins were made of Inconel 718 hardened to Rc45. The upper pull rod was connected through a universal joint to improve axiality of loading. The tests were conducted at a constant crosshead speed of 0.05 inch per minute throughout the test.

Deflection measurements were made with a linear variable displacement transducer (LVDT) extensometer. The extensometer knife edges were spring-loaded to the specimen and operated through specimen failure. The extensometer gage length is 1.00 inch. The extensometer is rated as Class B-2 per ASTM E83-67.

Elevated test temperatures were obtained with a three-zone electric resistance split-tube furnace with a 9-inch hot zone. All tests were conducted in air.

Because of the difficulty in remotely attaching a thermocouple directly to the specimen, the following procedure was used to monitor specimen temperature. Chromel-alumel thermocouples were inserted in shallow holes in the center and each end of the gage section of a dummy specimen and in each grip. In test configuration, with a slight load on the specimen, a plot of specimen temperature versus upper and lower grip and controller temperatures was developed over the range room temperature to 550°F (288°C). The upper grip was used to control the furnace temperature. During the actual testing the grip temperatures were used to obtain desired specimen temperatures. Experiments indicated that this method is accurate to plus or minus 2°F.

The yield load, ultimate load, fracture load, total elongation, and uniform elongation were determined directly from the load-extension curve. The yield strength, ultimate strength, and fracture strength were calculated using the original cross-sectional area. The final diameter and final gage length were determined from postfracture photographs. The fracture area used to calculate the fracture stress (true stress at fracture) and percent reduction in area was computed using the final diameter measurement.

5.2. CHARPY V-NOTCH IMPACT TEST RESULTS

The results of Charpy V-notch impact tests performed on the various materials contained in Capsule T irradiated at 2.20×10^{18} n/cm² are presented in Tables 5-1 through 5-8 and Figures 5-1 through 5-4. A summary of the transition temperature increases and upper shelf energy decreases for the Capsule T material is shown in Table 5-9.

Irradiation of vessel intermediate shell forging 05 material specimens (axial orientation) to 2.20×10^{18} n/cm² (Figure 5-1) resulted in both 30 and 50 ft-lb transition temperature increases of 25°F and an upper shelf energy decrease of 6 ft-lb. Irradiation of vessel intermediate shell forging 05 material (tangential orientation) to 2.20×10^{18} n/cm² (Figure 5-2) resulted in both 30 and 50 ft-lb transition temperature increases of 60°F and an upper shelf energy decrease of 16 ft-lb.

Weld metal irradiated to 2.20×10^{18} n/cm² (Figure 5-3) resulted in both 30 and 50 ft-lb transition temperature increases of 80°F and 75°F, respectively, and an upper shelf energy decrease of 2 ft-lb.

Weld HAZ metal irradiated to 2.20×10^{18} n/cm² (Figure 5-4) resulted in both 30 and 50 ft-lb transition temperature increases of 50°F respectively and an upper shelf energy decrease of 2 ft-lb.

The fracture appearance of each irradiated Charpy specimen from the various materials is shown in Figures 5-5 through 5-8 and show an increasing ductile or tougher appearance with increasing test temperature.

Figure 5-9 shows a comparison of the 30 ft-lb transition temperature increases for the various Sequoyah Unit 2 surveillance materials with predicted increases using the methods of NRC Regulatory Guide 1.99, Revision 1.⁽³⁾ This comparison shows that the transition temperature increases resulting from irradiation to 2.20×10^{18} n/cm² are less than predicted by the Guide for the axial and tangential orientations of forging 05. The weld metal transition temperature increase resulting from 2.20×10^{18} n/cm² is greater than predicted by the Guide. Therefore, a trend line passing through the actual increase in transition temperature as determined from the irradiated weld specimens was used to set future operating limits for the vessel (Appendix A).

5-3. TENSION TEST RESULTS

The results of tension tests performed on forging 05 (axial orientation) and weld metal irradiated to 2.20×10^{18} n/cm² are shown in Table 5-10 and Figures 5-10 and 5-11, respectively. These results show that irradiation produced an increase in 0.2 percent yield strength of 7 to 8 ksi for forging 05 and approximately 6 ksi for the weld metal. Fractured tension specimens for each of the materials are shown in Figure 5-12. A typical stress-strain curve for the tension specimens is shown in Figure 5-13.

5-4. WELD OPENING LOADING TESTS .

Test results for weld opening loading (WOL) fracture mechanics specimens contained in Capsule T will be reported at a later time.

TABLE 5-1

CHARPY V-NOTCH IMPACT DATA FOR THE SEQUOYAH UNIT 2
 INTERMEDIATE SHELL FORGING 05 (AXIAL ORIENTATION)
 IRRADIATED AT 550°F, FLUENCE 2.20×10^{18} n/cm² (E > 1 MeV)

Sample No.	Temperature		Impact Energy		Lateral Expansion		Shear (%)
	C	(F)	Joules	(ft-lb)	MM	(mils)	
NT54	-32	(-25)	24.5	(18.0)	0.42	(16.5)	7
NT55	-18	(0)	36.5	(27.0)	0.62	(24.5)	12
NT53	-4	(25)	39.5	(29.0)	0.58	(23.0)	18
NT52	-4	(25)	27.0	(20.0)	0.51	(20.0)	16
NT59*	10	(50)					
NT50	24	(75)	51.5	(38.0)	0.90	(35.5)	43
NT60	24	(75)	47.5	(35.0)	0.85	(33.5)	31
NT56	38	(100)	87.0	(64.0)	1.40	(55.0)	70
NT58	66	(150)	101.5	(75.0)	1.45	(57.0)	94
NT51	93	(200)	110.0	(81.0)	1.50	(59.0)	100
NT49	121	(250)	111.0	(82.0)	1.82	(71.5)	100
NT57	149	(300)	114.0	(84.0)	1.68	(66.0)	100

*Specimen was not centered on Anvil

TABLE 5-2

CHARPY V-NOTCH IMPACT DATA FOR THE SEQUOYAH UNIT 2
 INTERMEDIATE SHELL FORGING 05 (TANGENTIAL ORIENTATION)
 IRRADIATED AT 550°F, FLUENCE 2.20×10^{18} n/cm² (E > 1 MeV)

Sample No.	Temperature		Impact Energy		Lateral Expansion		Shear (%)
	C	(F)	Joules	(ft-lb)	MM	(mils)	
NL38	-46	(-50)	12.0	(9.0)	0.19	(7.5)	3
NL36	-32	(-25)	12.0	(9.0)	0.23	(9.0)	5
NL33	-18	(0)	55.5	(41.0)	0.71	(28.0)	18
NL35	-4	(25)	69.0	(51.0)	1.00	(39.5)	28
NL34	38	(100)	88.0	(65.0)	1.26	(49.5)	50
NL37	66	(150)	143.5	(106.0)	1.96	(77.0)	85
NL39	93	(200)	161.5	(119.0)	2.10	(82.5)	100
NL40	149	(300)	158.5	(117.0)	2.26	(89.0)	100

TABLE 5-3

CHARPY V-NOTCH IMPACT DATA FOR THE SEQJOYAH UNIT 2
 PRESSURE VESSEL WELD METAL IRRADIATED AT 550°F,
 FLUENCE 2.20×10^{18} n/cm² (E > 1 MeV)

Sample No.	Temperature		Impact Energy		Lateral Expansion		Shear (%)
	C	(F)	Joules	(ft-lb)	MM	(mils)	
W58	-32	(-25)	51.5	(38.0)	0.85	(33.5)	48
W49	-32	(-25)	85.5	(63.0)	1.21	(47.5)	25
W53	-18	(-0)	19.0	(14.0)	0.29	(11.5)	24
W55	-4	(25)	42.0	(31.0)	0.72	(28.5)	29
W50	-4	(25)	20.5	(15.0)	0.42	(16.5)	25
W52	10	(50)	130.0	(96.0)	2.17	(85.5)	96
W54	24	(75)	96.5	(71.0)	1.51	(59.5)	48
W59	38	(100)	42.0	(31.0)	0.67	(26.5)	55
W60	52	(125)	154.5	(114.0)	2.25	(88.5)	100
W51	66	(150)	153.0	(113.0)	2.13	(84.0)	100
W56	93	(200)	158.5	(117.0)	2.17	(85.5)	100
W57	149	(300)	133.0	(98.0)	2.16	(85.0)	100

TABLE 5-4

CHARPY V-NOTCH IMPACT DATA FOR THE SEQUOYAH UNIT 2
 PRESSURE VESSEL WELD HEAT AFFECTED ZONE METAL
 IRRADIATED AT 550°F, FLUENCE 2.20×10^{18} n/cm² (E > 1 MeV)

Sample No.	Temperature		Impact Energy		Lateral Expansion		Shear (%)
	C	(F)	Joules	(ft-lb)	MM	(mils)	
H50	-32	(-25)	28.5	(21.0)	0.33	(13.0)	11
H51	-18	(-0)	55.5	(41.0)	0.75	(29.5)	49
H49	-18	(0)	80.0	(59.0)	0.76	(30.0)	69
H53	-4	(25)	81.5	(60.0)	1.03	(40.5)	66
H59	10	(50)	96.5	(71.0)	1.21	(47.5)	67
H54	24	(75)	111.0	(82.0)	1.38	(54.5)	78
H60	38	(100)	152.0	(112.0)	1.64	(64.5)	93
H57	52	(125)	57.0	(42.0)	0.91	(36.0)	63
H52	66	(150)	161.5	(119.0)	1.94	(76.5)	99
H56	93	(200)	162.5	(120.0)	1.83	(72.0)	100
H55	149	(300)	167.0	(123.0)	1.93	(76.0)	100
H58	149	(300)	118.0	(87.0)	1.85	(73.0)	100

TABLE 5-5

**INSTRUMENTED CHARPY IMPACT TEST RESULTS FOR
SEQUOYAH UNIT 2 INTERMEDIATE SHELL
FORGING 05 (AXIAL ORIENTATION)**

Sample No.	Test Temp. (°C)	Charpy Energy (Joules)	Normalized Energies			Yield Load (N)	Time to Yield (μSec)	Maximum Load (N)	Time to Maximum (μSec)	Fracture Load (N)	Arrest Load (N)	Yield Stress (MPa)	Flow Stress (MPa)
			Charpy Ed/A (kJ/m ²)	Maximum Em/A (kJ/m ²)	Prop Ep/A (kJ/m ²)								
NT54	-32	24.5	305	237	68	14,000	90	17,600	285	17,000	0	719	811
NT55	-18	36.5	458	369	88	13,900	125	18,500	450	18,000	0	714	832
NT52	-4	27.0	339	198	141	13,500	85	16,100	260	15,900	400	692	760
NT53	-4	39.5	491	388	103	15,100	90	18,500	420	18,500	100	776	865
NT59	10												
NT60	24	47.5	593	384	209	14,400	100	18,600	430	18,200	4200	740	848
NT50	24	51.5	644	376	268	14,100	90	18,000	425	18,000	4100	728	826
NT56	38	87.0	1085	470	614	14,600	90	19,000	500	17,200	8300	751	865
NT58	66	101.5	1271	460	811	14,200	90	18,600	500	13,800	8900	729	843
NT51	93	110.0	1373	430	943	12,800	95	17,500	510	11,700	8400	656	779
NT49	121	111.0	1390	411	978	10,800	90	16,700	520			555	707
NT57	149	114.0	1424	436	987	11,200	70	17,700	505			575	743

TABLE 5-6

INSTRUMENTED CHARPY IMPACT TEST RESULTS FOR
SEQUOYAH UNIT 2 INTERMEDIATE SHELL
FORGING 05 (TANGENTIAL ORIENTATION)

Sample No.	Test Temp. (°C)	Charpy Energy (Joules)	Normalized Energies			Yield Load (N)	Time to Yield (µSec)	Maximum Load (N)	Time to Maximum (µSec)	Fracture Load (N)	Arrest Load (N)	Yield Stress (MPa)	Flow Stress (MPa)
			Charpy Ed/A (kJ/m²)	Maximum Em/A (kJ/m²)	Prop Ep/A (kJ/m²)								
NL38	-46	12.0	153	82	70	15,500	90	16,700	125	16,900	0	795	827
NL36	-32	12.0	153	82	70	14,700	85	15,700	125	15,600	0	754	780
NL33	-18	55.5	695	602	93	16,400	90	20,800	580	20,700	0	844	957
NL35	-4	69.0	864	539	325	14,100	100	19,000	585	18,300	0	726	853
NL34	38	88.0	1102	613	489	14,200	90	19,200	645	19,000	5600	731	859
NL37	66	143.5	1796	601	1195	13,200	85	18,500	655	13,800	8900	678	816
NL39	93	161.5	2017	577	1440	13,100	90	18,200	640			672	805
NL40	149	158.5	1983	729	1254	11,100	120	16,700	700			572	715

TABLE 5-7

**INSTRUMENTED CHARPY IMPACT TEST RESULTS FOR
SEQUOYAH UNIT 2 WELD METAL**

Sample No.	Test Temp. (°C)	Charpy Energy (Joules)	Normalized Energies			Yield Load (N)	Time to Yield (μSec)	Maximum Load (N)	Time to Maximum (μSec)	Fracture Load (N)	Arrest Load (N)	Yield Stress (MPa)	Flow Stress (MPa)
			Charpy Ed/A (kJ/m ²)	Maximum Em/A (kJ/m ²)	Prop Ep/A (kJ/m ²)								
W49	-32	85.5	1068	577	491	15,400	95	19,100	600	18,100	200	791	887
W58	-32	51.5	644	515	129	13,700	80	17,700	570	17,600	0	706	808
W53	-18	19.0	237	197	41	14,900	85	17,100	235	17,100	100	765	823
W50	-4	20.5	254	192	62	13,400	85	15,800	250	15,800	1200	688	751
W55	-4	42.0	525	377	148	13,900	115	17,800	445	17,100	0	713	815
W52	10	130.0	1627	593	1034	13,300	100	17,800	675	10,700	0	683	800
W54	24	96.5	1203	595	603	13,300	125	17,800	700	14,800	2600	685	801
W59	38	42.0	525	383	143	13,400	85	17,000	445	16,900	4300	688	731
W60	52	154.5	1932	622	1310	11,800	90	16,100	765			605	718
W51	66	153.0	1915	574	1341	11,900	80	16,800	675			613	738
W56	93	158.5	1983	624	1359	12,300	90	17,700	705			635	771
W57	149	133.0	1661	480	1181	10,000	85	14,600	655			516	634

TABLE 5-8

**INSTRUMENTED CHARPY IMPACT TEST RESULTS FOR
SEQUOYAH UNIT 2 WELD HEAT AFFECTED ZONE METAL**

Sample No.	Test Temp. (°C)	Charpy Energy (Joules)	Normalized Energies			Yield Load (N)	Time to Yield (μSec)	Maximum Load (N)	Time to Maximum (μSec)	Fracture Load (N)	Arrest Load (N)	Yield Stress (MPa)	Flow Stress (MPa)
			Charpy Ed/A (kJ/m ²)	Maximum Em/A (kJ/m ²)	Prop Ep/A (kJ/m ²)								
H50	-32	28.5	356	337	19	16,900	90	20,600	335	20,600	0	869	964
H49	-18	80.0	1000	693	307	10,300	90	21,100	665	20,700	5900	840	962
H51	-18	55.5	695	397	298	15,700	105	19,500	430	19,400	5000	809	906
H53	-4	81.5	1017	527	490	14,000	85	19,000	560	17,000	200	718	848
H59	10	96.5	1203	482	721	15,300	90	19,400	500	18,100	9100	786	893
H54	24	111.0	1390	555	834	14,800	90	19,500	575	12,000	5500	763	882
H60	38	152.0	1898	628	1270	15,200	90	20,200	630	13,700	6200	782	910
H57	52	57.0	712	472	240	14,500	95	19,200	505	18,700	4900	748	869
H52	66	161.5	2017	632	1384	13,800	90	19,500	665			712	858
H56	93	162.5	2034	739	1295	13,600	85	19,900	755			702	864
H58	149	118.0	1474	481	994	10,500	85	16,700	585			540	700
H55	149	167.0	2085	643	1441	13,100	95	18,200	715			674	805

TABLE 5-9

EFFECT OF 550°F IRRADIATION AT 2.20×10^{18} ($E > 1$ MeV)
ON THE NOTCH TOUGHNESS PROPERTIES OF THE
SEQUOYAH UNIT 2 REACTOR VESSEL MATERIALS

Material	Average 30 ft-lb Temp (°F)			Average 35 mil Lateral Expansion Temp (°F)			Average 50 ft-lb Temp (°F)			Average Energy Absorption at Full Shear (ft-lb)		
	Unirradiated	Irradiated	ΔT	Unirradiated	Irradiated	ΔT	Unirradiated	Irradiated	ΔT	Unirradiated	Irradiated	Δ (ft-lb)
Forging 05 (Axial)	0	25	25	20	50	30	60	85	25	88	82	6
Forging 05 (Tangential)	-70	-10	60	-45	20	65	-25	35	60	134	118	16
Weld Metal	-75	5	80	-50	15	65	-40	35	75	112	110	2
HAZ Metal	-60	-10	50	-25	15	40	-30	20	50	122	120	2

TABLE 5-10

**TENSILE PROPERTIES FOR SEQUOYAH UNIT 2
REACTOR VESSEL MATERIAL IRRADIATED TO 2.20×10^{18} n/cm²**

Sample No.	Material	Test Temp (°F)	.2% Yield Strength (ksi)	Ultimate Strength (ksi)	Fracture Load (kip)	Fracture Stress (ksi)	Fracture Strength (ksi)	Uniform Elongation (%)	Total Elongation (%)	Reduction in Area (%)
NT9	Forging 05 (Axial)	200	66.6	84.5	2.95	158.4	60.1	9.7	20.2	62
NT10	Forging 05 (Axial)	550	61.5	86.0	3.30	147.1	57.2	9.5	18.4	54
W10	Weld Metal	150	68.2	82.5	2.72	221.6	55.4	9.0	21.0	75
W9	Weld Metal	550	63.2	80.3	3.10	170.8	63.2	7.8	16.0	63

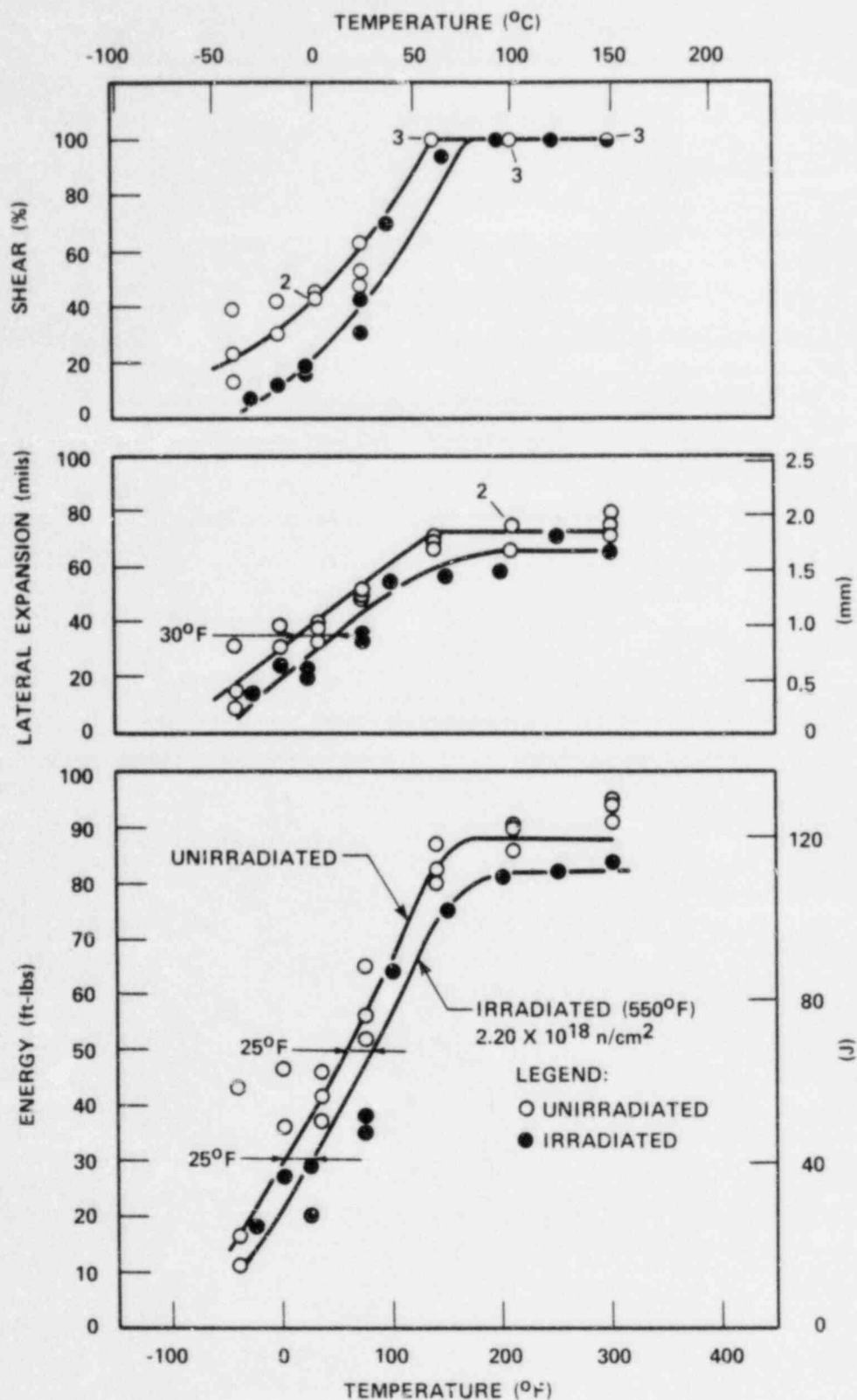


Figure 5-1. Irradiated Charpy V-Notch Impact Properties for Sequoyah Unit 2 Reactor Vessel Intermediate Shell Forging 05 (Axial Orientation)

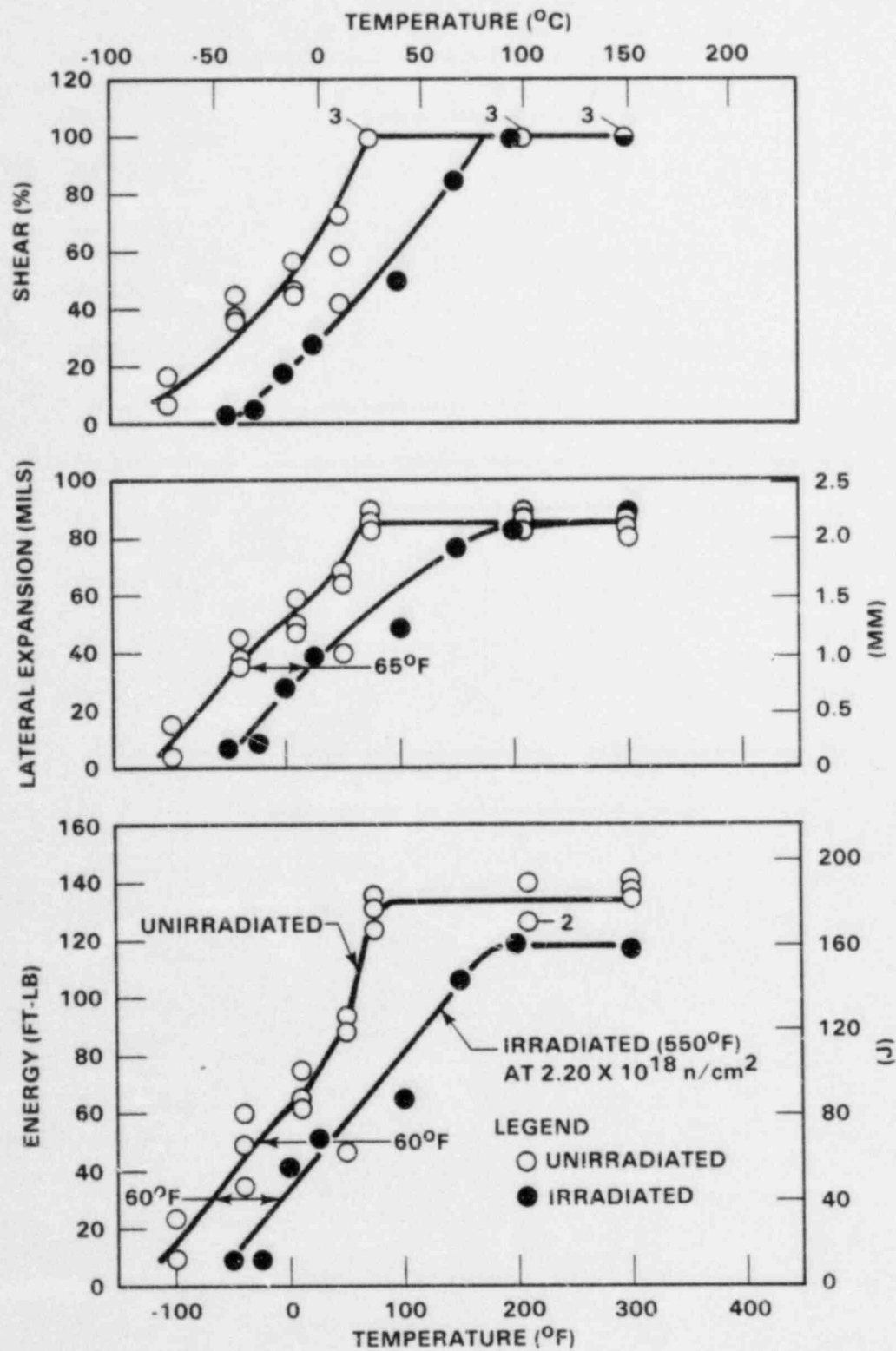


Figure 5-2. Irradiated Charpy V-Notch Impact Properties for Sequoyah Unit 2 Reactor Vessel Intermediate Shell Forging 05 (Tangential Orientation)

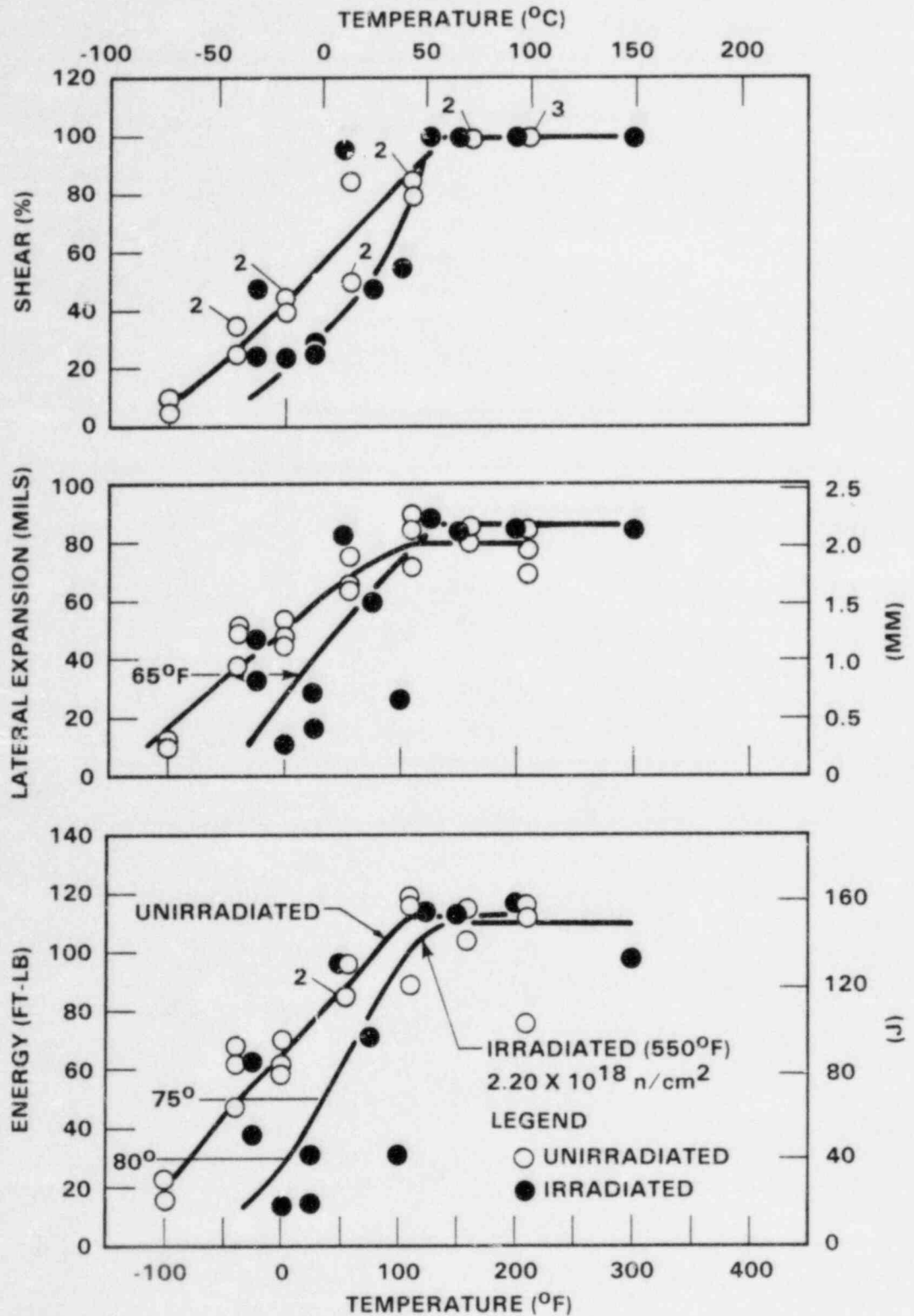


Figure 5-3. Irradiated Charpy V-Notch Impact Properties for Sequoyah Unit 2 Reactor Pressure Vessel Weld Metal

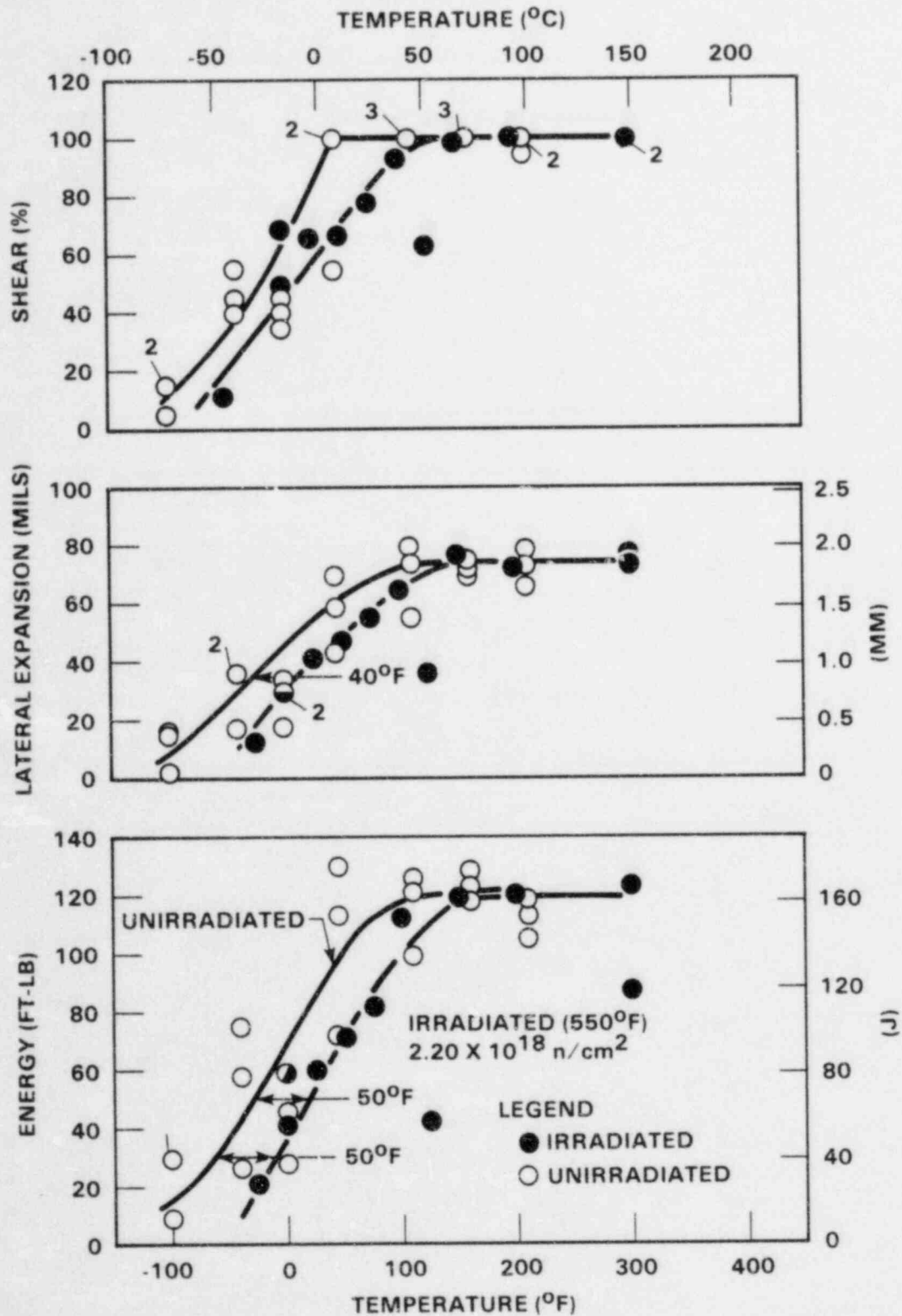


Figure 5-4. Irradiated Charpy V-Notch Impact Properties for Sequoyah Unit 2 Reactor Pressure Vessel Weld Heat Affected Zone Metal

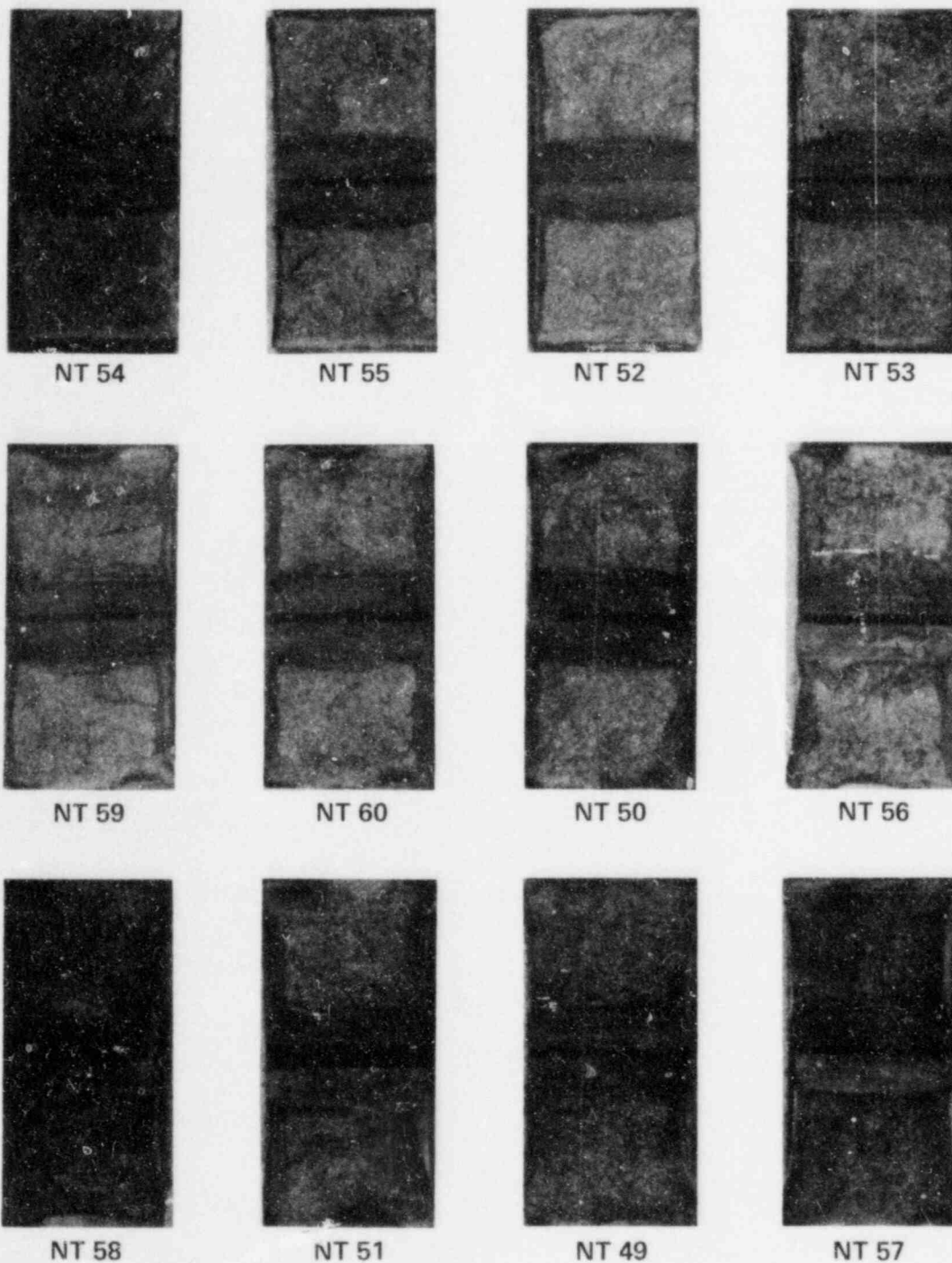


Figure 5-5. Charpy Impact Specimen Fracture Surfaces for Sequoyah Unit 2 Pressure Vessel Intermediate Shell Forging 05 (Axial Orientation)

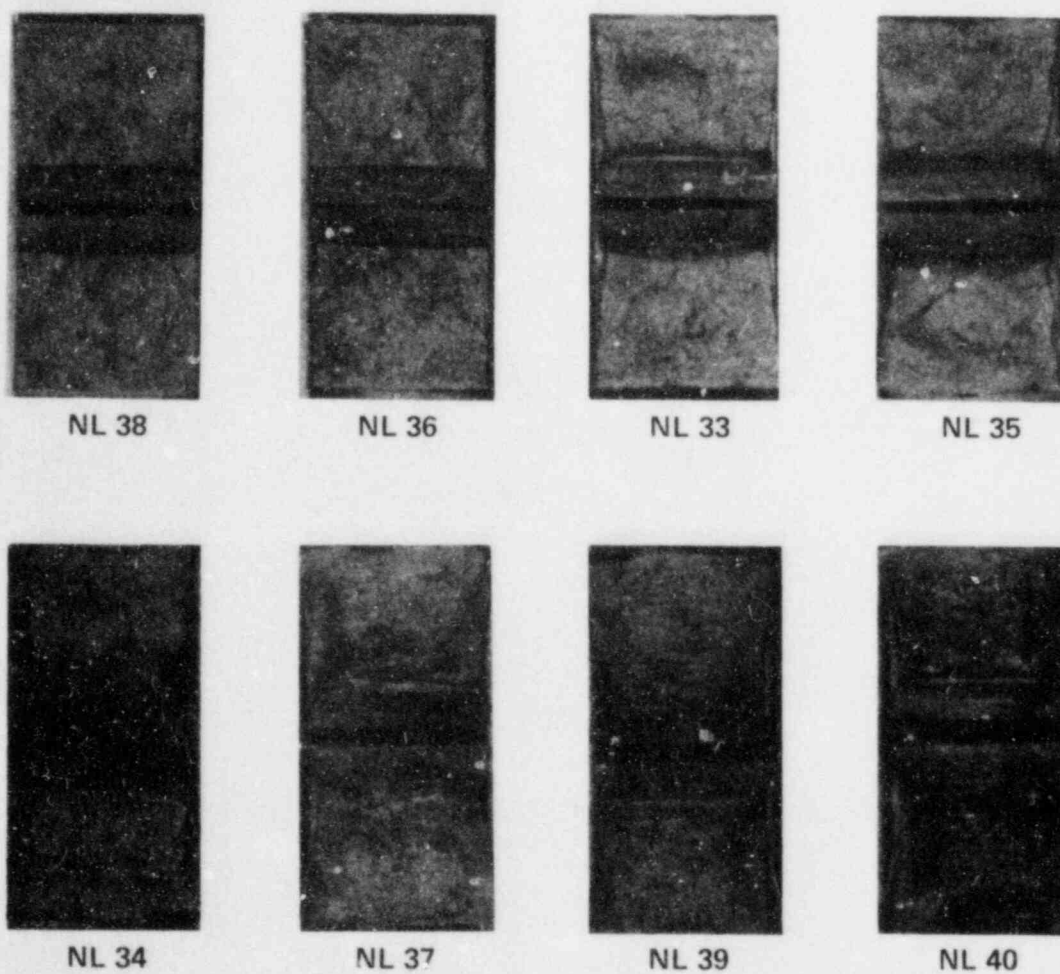


Figure 5-6. Charpy Impact Specimen Fracture Surfaces for Sequoyah Unit 2 Pressure Vessel Intermediate Shell Forging 05 (Tangential Orientation)

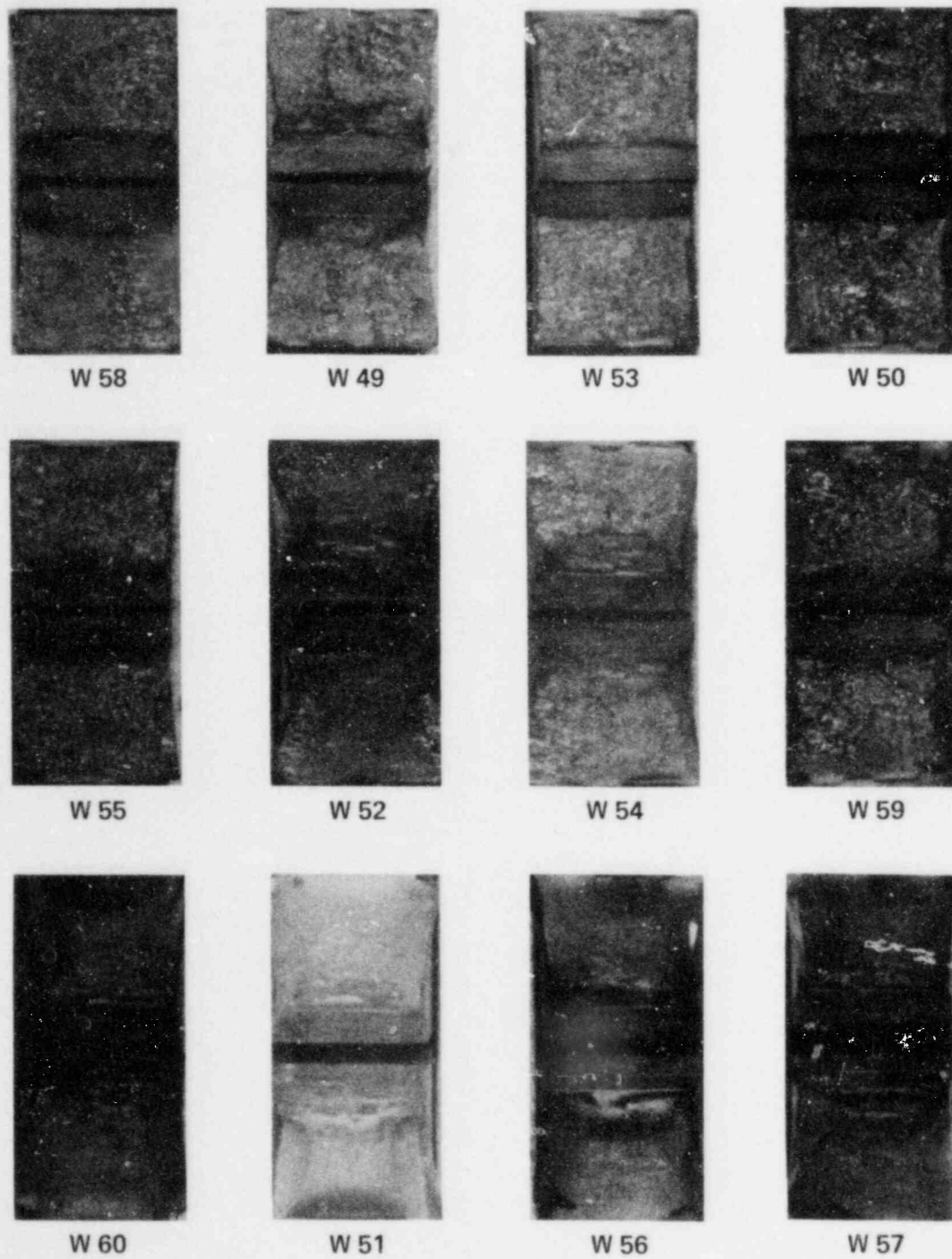


Figure 5-7. Charpy Impact Specimen Fracture Surfaces for Sequoyah Unit 2 Weld Metal

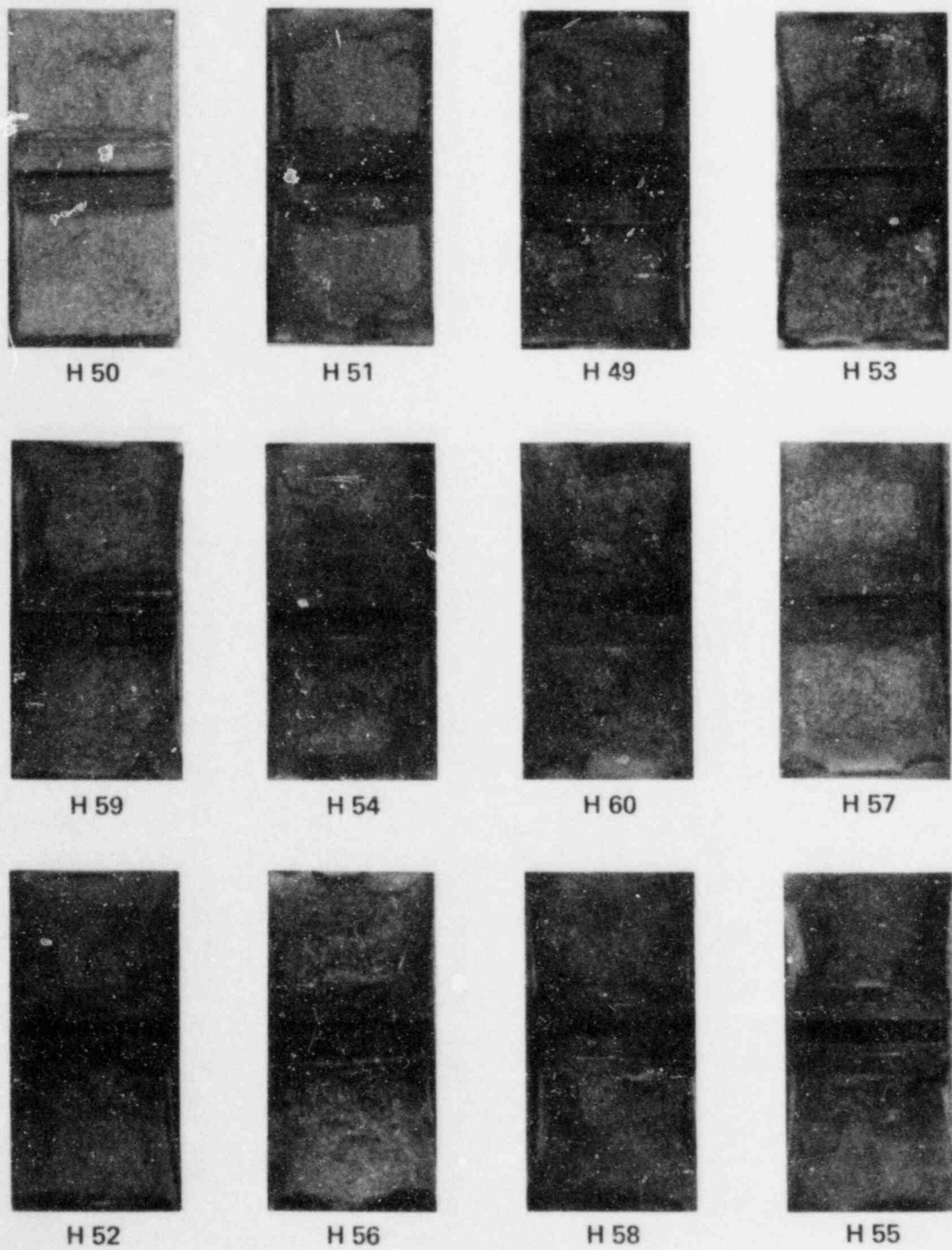


Figure 5-8. Charpy Impact Specimen Fracture Surfaces for Sequoyah Unit 2 Weld Heat Affected Zone Metal

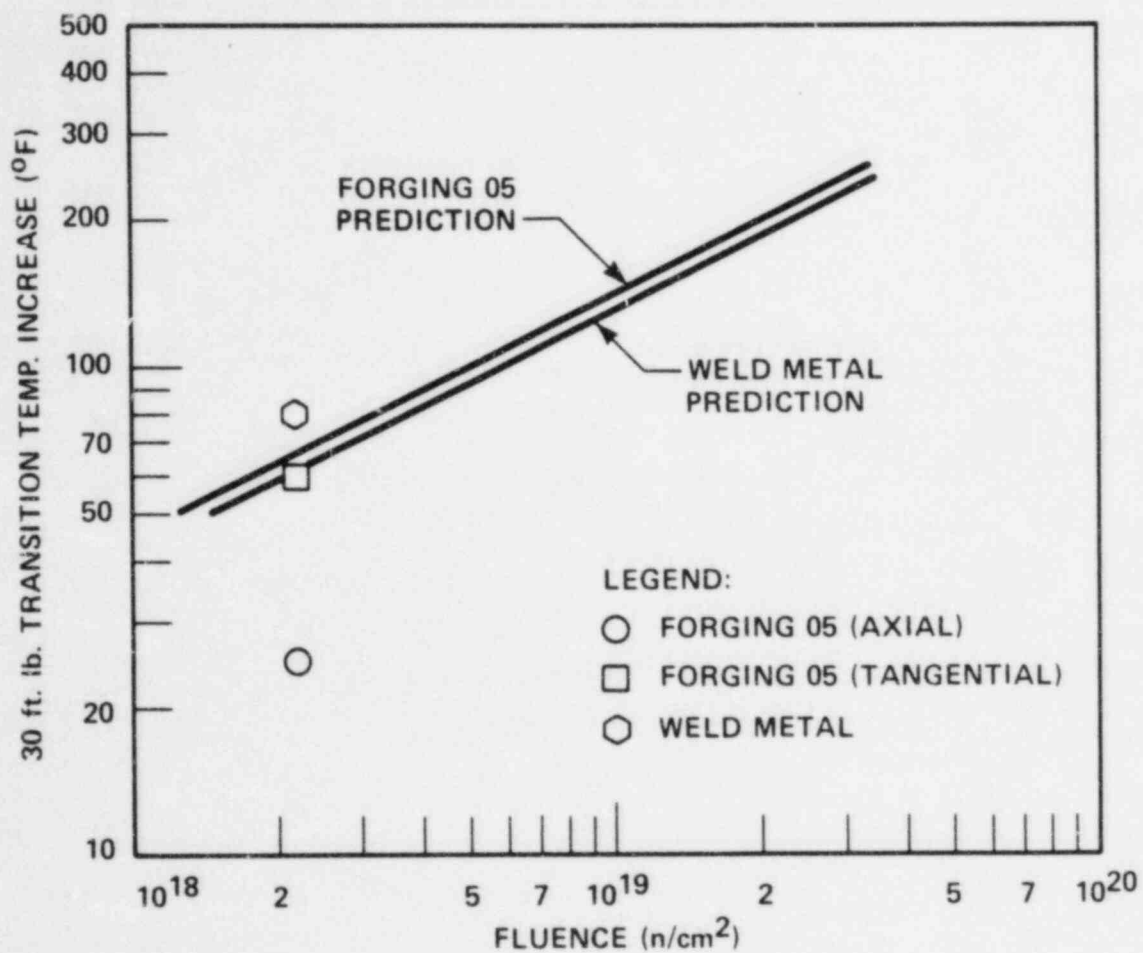


Figure 5-9. Comparison of Actual versus Predicted 30 ft-lb Transition Temperature Increases for the Sequoyah Unit 2 Reactor Vessel Material Based on the Prediction Methods of Regulatory Guide 1.99 Revision 1

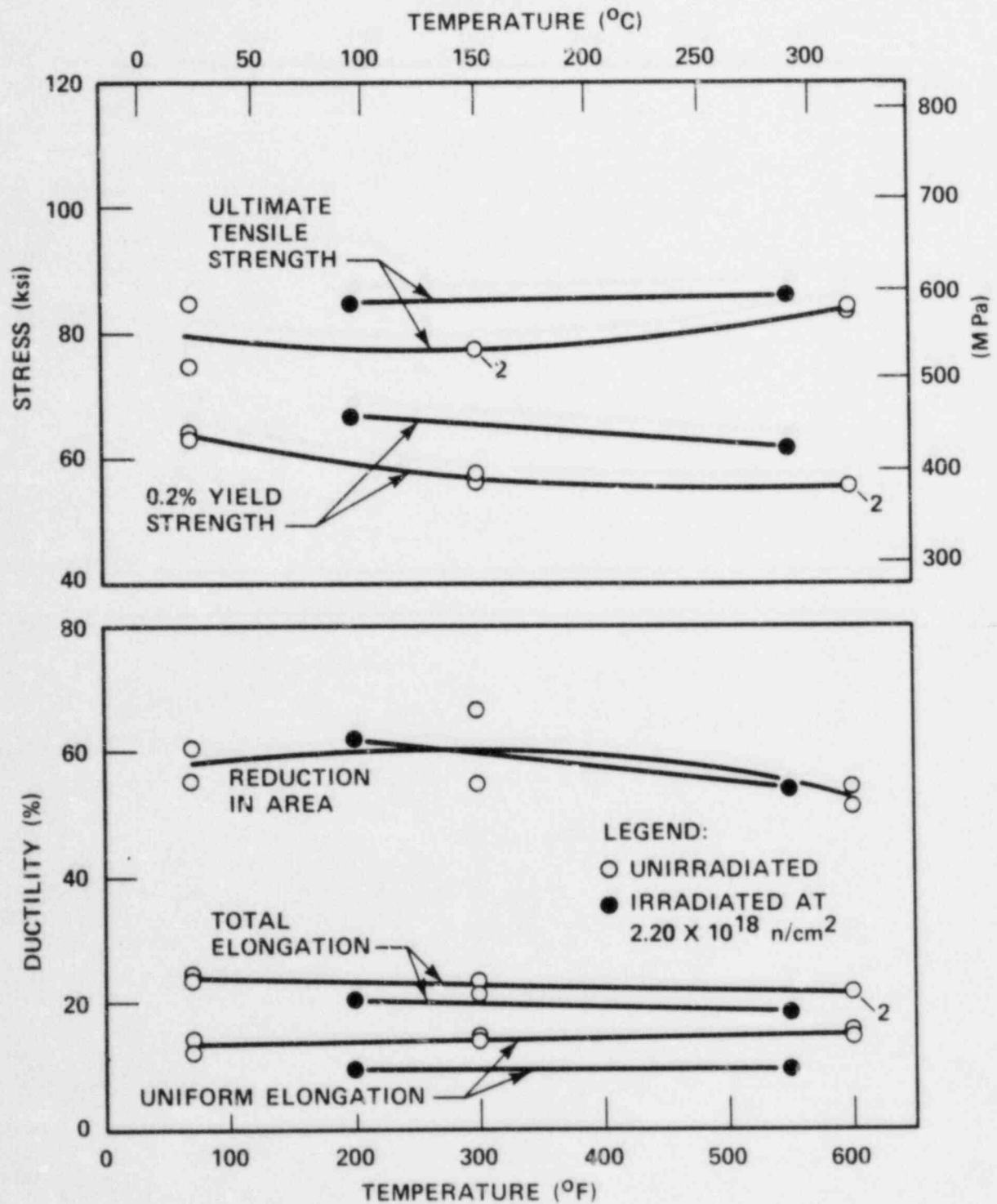


Figure 5-10. Tensile Properties for Sequoyah Unit 2 Reactor Vessel Intermediate Shell Forging 05 (Axial Orientation)

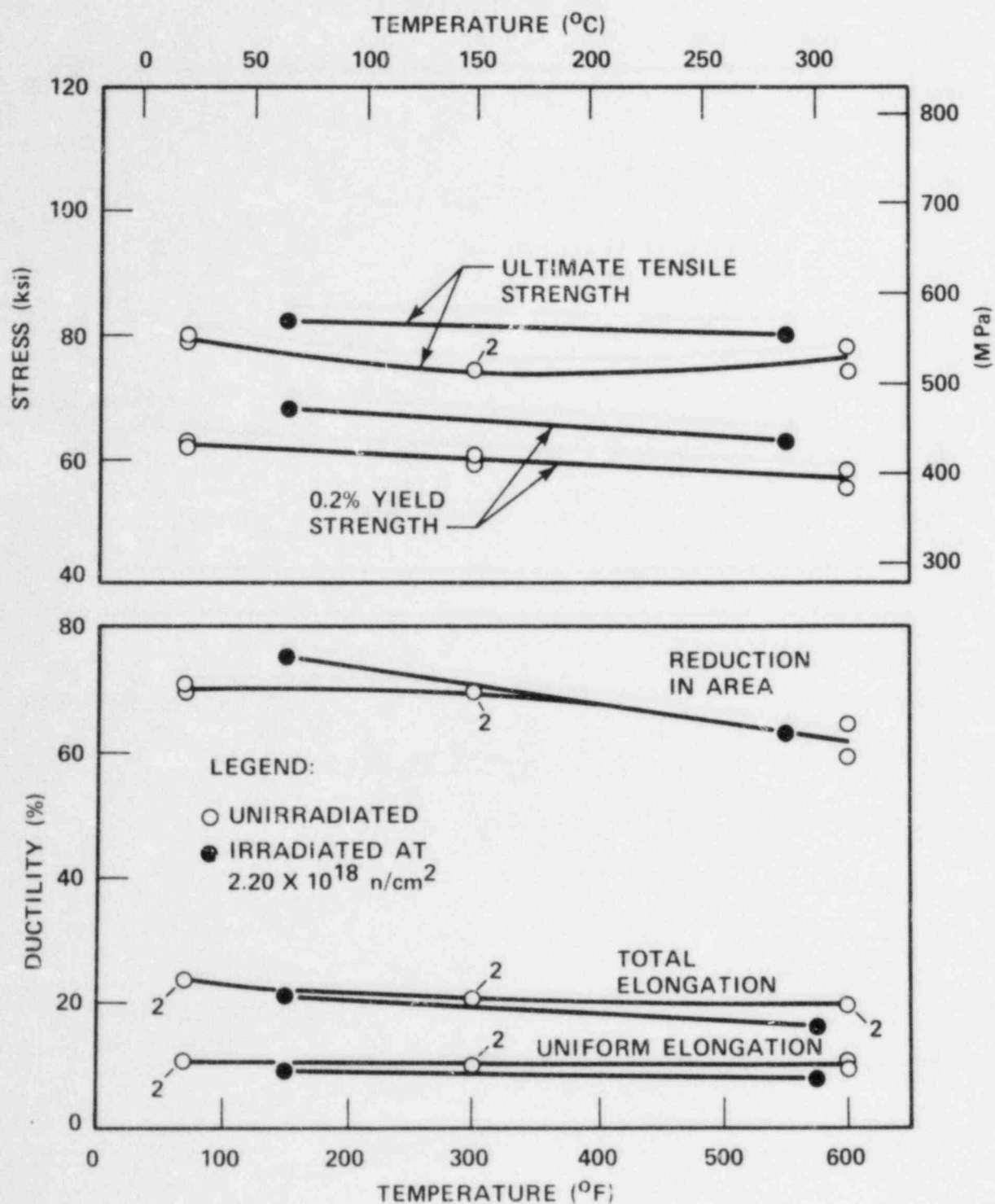


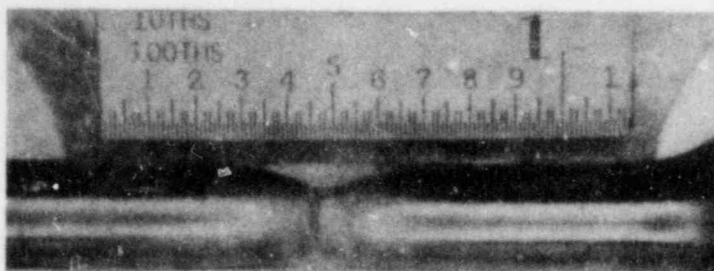
Figure 5-11. Tensile Properties for Sequoyah Unit 2 Reactor Vessel Weld Metal



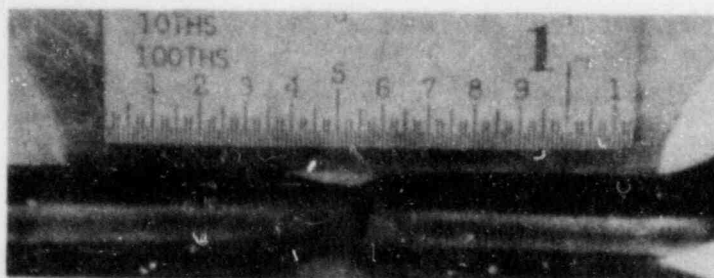
TENSILE SPECIMEN NT 9
TESTED AT 200°F



TENSILE SPECIMEN NT 10
TESTED AT 550°F



TENSILE SPECIMEN W 10
TESTED AT 150°F



TENSILE SPECIMEN W 9
TESTED AT 550°F

Figure 5-12. Fractured Tensile Specimens of Sequoyah Unit 2 Reactor Vessel Intermediate Shell Forging 05 (Axial Orientation) and Weld Metal

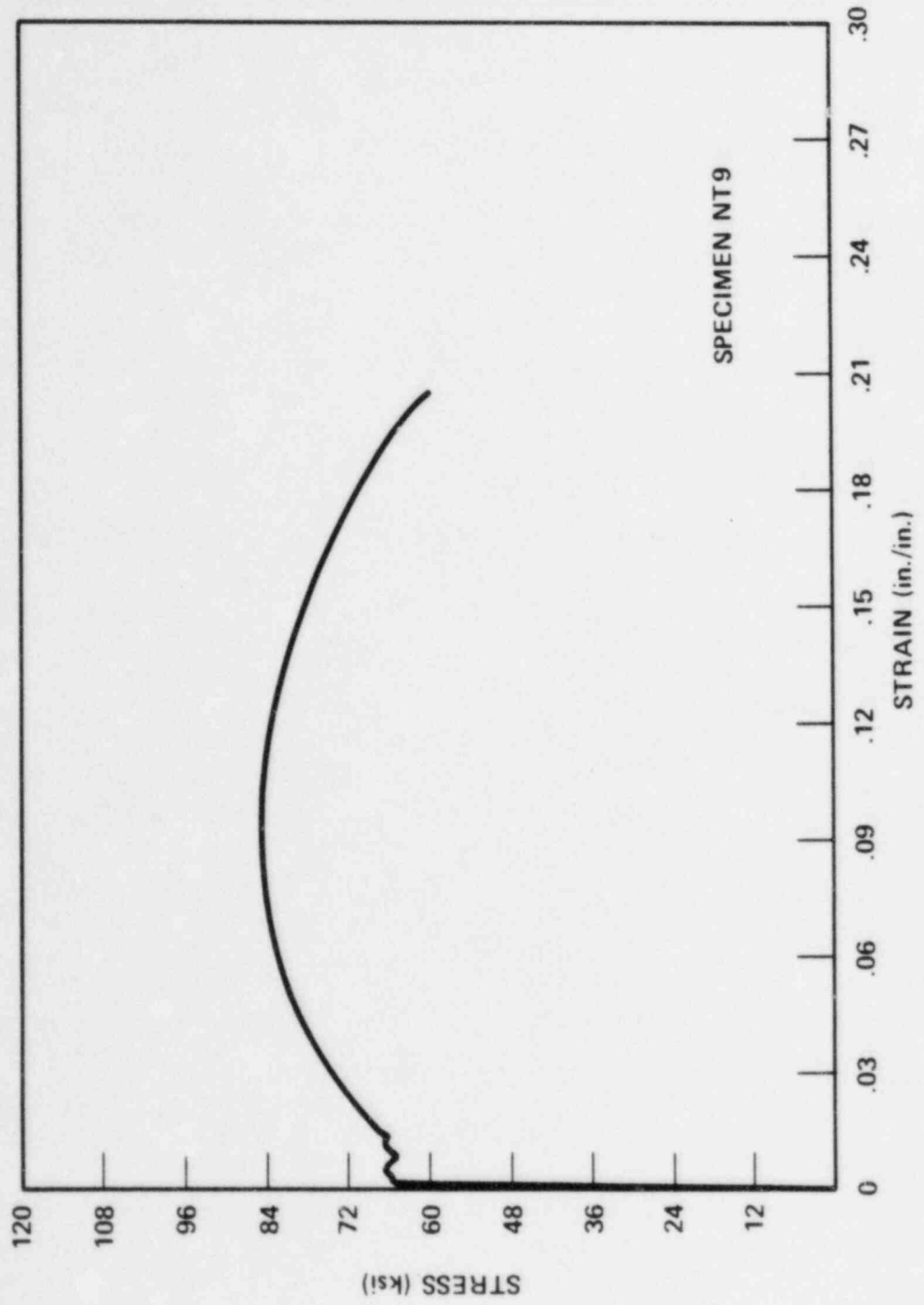


Figure 5-13. Typical Stress-Strain Curve for Tensile Specimens

SECTION 6

RADIATION ANALYSIS AND NEUTRON DOSIMETRY

6-1. INTRODUCTION

Knowledge of the neutron environment within the pressure vessel/surveillance capsule geometry is required as an integral part of LWR pressure vessel surveillance programs for two reasons. First, in the interpretation of radiation-induced properties, changes observed in materials test specimens and the neutron environment (fluence, flux) to which the test specimens were exposed must be known. Second, in relating the changes observed in the test specimens to the present and future condition of the reactor pressure vessel, a relationship must be established between the environment at various positions within the reactor vessel and that experienced by the test specimens. The former requirement is normally met by employing a combination of rigorous analytical techniques and measurements obtained with passive neutron flux monitors contained in each of the surveillance capsules. The latter information is derived solely from analysis.

This section describes a discrete ordinates S_n transport analysis performed for the Sequoyah Unit 2 reactor to determine the fast neutron ($E > 1.0$ MeV) flux and fluence as well as the neutron energy spectra within the reactor vessel and surveillance capsules. The analytical data were then used to develop lead factors for use in relating neutron exposure of the pressure vessel to that of the surveillance capsules. Based on spectrum-averaged reaction cross sections derived from this calculation, the analysis of the neutron dosimetry contained in Capsule T is discussed and comparisons with analytical predictions are presented.

6-2. DISCRETE ORDINATES ANALYSIS

A plan view of the Sequoyah Unit 2 reactor geometry at the core midplane is shown in Figure 6-1. Since the reactor exhibits 1/8th core symmetry, only a zero- to 45-degree sector is depicted. Eight irradiation capsules attached to the thermal shield are included in the design to constitute the reactor vessel surveillance program. Four capsules are located symmetrically at 4 and 40 degrees from the cardinal axes as shown in Figure 6-1.

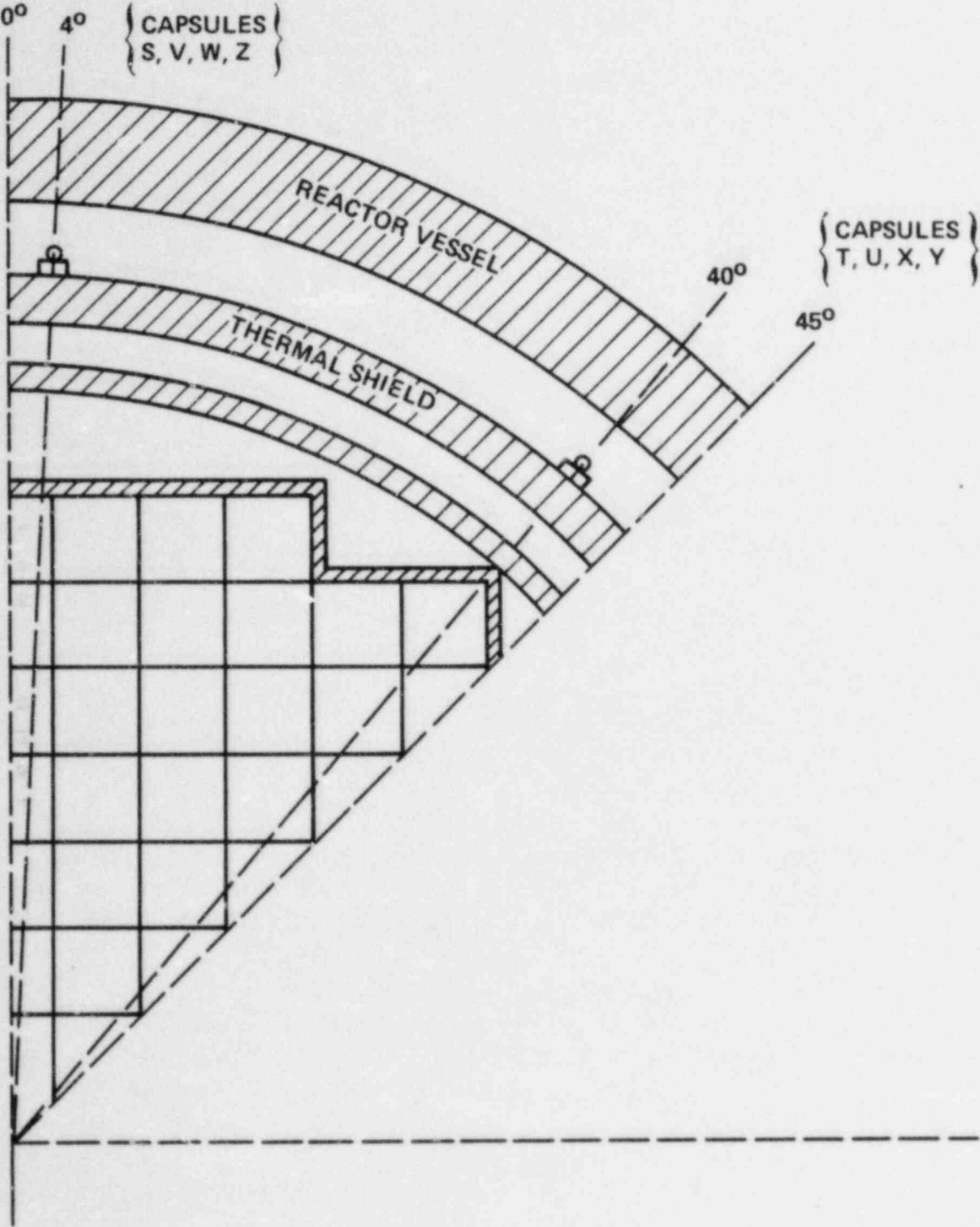


Figure 6-1. Sequoyah Unit 2 Reactor Geometry

A plan view of a single surveillance capsule attached to the thermal shield is shown in Figure 6-2. The stainless steel specimen container is 1-inch square and approximately 38 inches in height. The containers are positioned axially such that the specimens are centered on the core midplane, thus spanning the central 3 feet of the 12-foot-high reactor core.

From a neutronic standpoint, the surveillance capsule structures are significant. In fact, as is shown later, they have a marked effect on the distributions of neutron flux and energy spectra in the water annulus between the thermal shield and the reactor vessel. Thus, in order to properly ascertain the neutron environment at the test specimen locations, the capsules themselves must be included in the analytical model. Use of at least a two-dimensional computation is therefore mandatory.

In the analysis of the neutron environment within the Sequoyah Unit 2 reactor geometry, predictions of neutron flux magnitude and energy spectra were made with the DOT⁽⁴⁾ two-dimensional discrete ordinates code. The radial and azimuthal distributions were obtained from an R,θ computation wherein the geometry shown in Figures 6-1 and 6-2 was described in the analytical model. In addition to the R,θ computation, a second calculation in R,Z geometry was also carried out to obtain relative axial variations of neutron flux throughout the geometry of interest. In the R,Z analysis, the reactor core was treated as an equivalent volume cylinder and, of course, the surveillance capsules were not included in the model.

Both the R,θ and R,Z analyses employed 47 neutron energy groups and a P_3 expansion of the scattering cross sections. The cross sections used in the analyses were obtained from the SAILOR cross section library⁽⁵⁾ which was developed specifically for light water reactor applications. The neutron energy group structure used in the analysis is listed in Table 6-1.

A key input parameter in the analysis of the integrated fast neutron exposure of the reactor vessel is the core power distribution. For this analysis, power distributions representative of time-averaged conditions derived from statistical studies of long-term operation of Westinghouse 4-loop plants were employed. These input distributions include rod-by-rod spatial variations for all peripheral fuel assemblies.

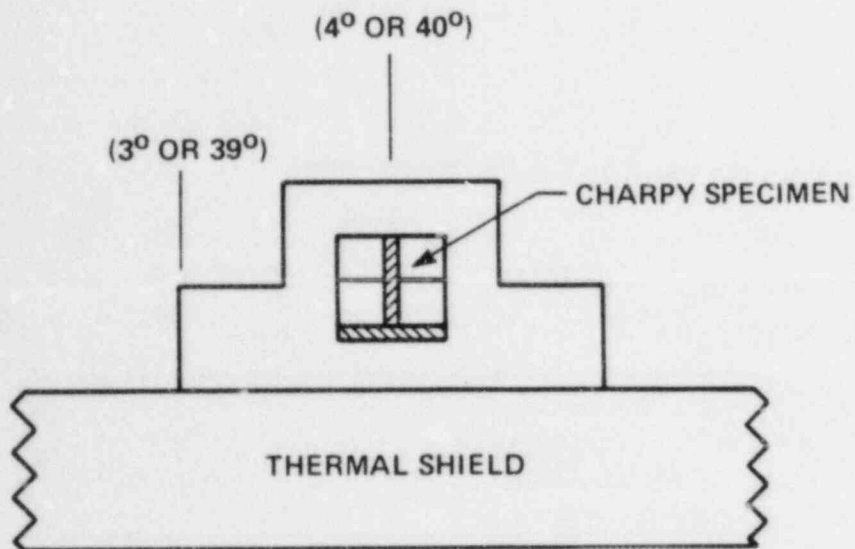


Figure 6-2. Plan View of a Reactor Vessel Surveillance Capsule

TABLE 6-1
47 GROUP ENERGY STRUCTURE

Group	Lower Energy (MeV)	Group	Lower Energy (MeV)
1	14.19 ^(a)	25	0.183
2	12.21	26	0.111
3	10.00	27	0.0674
4	8.61	28	0.0409
5	7.41	29	0.0318
6	6.07	30	0.0261
7	4.97	31	0.0242
8	3.68	32	0.0219
9	3.01	33	0.0150
10	2.73	34	7.10×10^{-3}
11	2.47	35	3.36×10^{-3}
12	2.37	36	1.59×10^{-3}
13	2.35	37	4.54×10^{-4}
14	2.23	38	2.14×10^{-4}
15	1.92	39	1.01×10^{-4}
16	1.65	40	3.73×10^{-5}
17	1.35	41	1.07×10^{-5}
18	1.00	42	5.04×10^{-6}
19	0.821	43	1.66×10^{-6}
20	0.743	44	8.76×10^{-7}
21	0.608	45	4.14×10^{-7}
22	0.498	46	1.00×10^{-7}
23	0.369	47	0.00
24	0.298		

[a] The upper energy of group 1 is 17.33 MeV.

It should be noted that this generic design basis power distribution is intended to provide a vehicle for long-term (end-of-life) projection of vessel exposure. Since plant-specific power distributions reflect only past operation, their use for projection into the future may not be justified; the use of generic data which reflects long-term operation of similar reactor cores may provide a more suitable approach.

Benchmark testing of these generic power distributions and the SAILOR cross sections against surveillance capsule data obtained from 2-loop and 4-loop Westinghouse plants indicate that this analytical approach yields conservative results, with calculations exceeding measurements from 10 to 25 percent.^[6]

One further point of interest regarding these analyses is that the design basis assumes an out-in fuel loading pattern (fresh fuel on the periphery). Future commitment to low-leakage loading patterns could significantly reduce the calculated neutron flux levels presented in Section 6-4. In addition, capsule lead factors could be changed, thereby influencing the withdrawal schedule of the remaining surveillance capsules.

Having the results of the R, θ and R,Z calculations, three-dimensional variations of neutron flux may be approximated by assuming that the following relation holds for the applicable regions of the reactor.

$$\phi(R,Z,\theta E_g) = \phi(R,\theta E_g) \times F(Z,E_g) \quad (6-1)$$

where

$\phi(R,Z,\theta E_g)$ = neutron flux at point R,Z, θ within energy group g

$\phi(R,\theta E_g)$ = neutron flux at point R, θ within energy group g obtained from the R, θ calculation

$F(Z,E_g)$ = relative axial distribution of neutron flux within energy group g obtained from the R,Z calculation

6-3 NEUTRON DOSIMETRY

The passive neutron flux monitors included in Capsule T of Sequoyah Unit 2 are listed in Table 6-2. The first five reactions in Table 6-2 are used as fast neutron monitors to relate neutron fluence ($E > 1.0$ MeV) to measured material property changes. To properly account for burnout of the product isotope generated by fast neutron reactions, it is necessary to also determine the magnitude of the thermal neutron flux at the monitor location. Therefore, bare and cadmium-covered cobalt-aluminum monitors were also included.

TABLE 6-2

NUCLEAR CONSTANTS FOR NEUTRON FLUX MONITORS CONTAINED IN
THE SEQUOYAH UNIT 2 SURVEILLANCE CAPSULES

Monitor Material	Reaction of Interest	Target Weight Fraction	Product Half-life	Fission Yield (%)
Copper	$\text{Cu}^{63} (n, \alpha) \text{Co}^{60}$	0.6917	5.27 years	
Iron	$\text{Fe}^{54} (n, p) \text{Mn}^{54}$	0.0585	314 days	
Nickel	$\text{Ni}^{58} (n, p) \text{Co}^{58}$	0.6777	71.4 days	
Uranium-238 ^[a]	$\text{U}^{238} (n, f) \text{Cs}^{137}$	1.0	30.2 years	6.3
Neptunium-237 ^[a]	$\text{Np}^{237} (n, f) \text{Cs}^{137}$	1.0	30.2 years	6.5
Cobalt-aluminum ^[a]	$\text{Co}^{59} (n, \gamma) \text{Co}^{60}$	0.0015	5.27 years	
Cobalt-aluminum	$\text{Co}^{59} (n, \gamma) \text{Co}^{60}$	0.0015	5.27 years	

[a] Denotes that monitor is cadmium-shielded

The relative locations of the various monitors within the surveillance capsule are shown in Figure 4-2. The iron, nickel, copper, and cobalt-aluminum monitors, in wire form, are placed in holes drilled in spacers at several axial levels within the capsules. The cadmium-shielded neptunium and uranium fission monitors are accommodated within the dosimeter block, located near the center of the capsule.

The use of passive monitors such as those listed in Table 6-2 does not yield a direct measure of the energy-dependent flux level at the point of interest. Rather, the activation or fission process is a measure of the integrated effect that the time- and energy-dependent neutron flux has on the target material over the course of the irradiation period. An accurate assessment of the average neutron flux level incident on the various monitors may be derived from the activation measurements only if the irradiation parameters are well known. In particular, the following variables are of interest.

- The operating history of the reactor
- The energy response of the monitor
- The neutron energy spectrum at the monitor location
- The physical characteristics of the monitor

The analysis of the passive monitors and subsequent derivation of the average neutron flux requires completion of two operations. First, the disintegration rate of product isotope per unit mass of monitor must be determined. Second, in order to define a suitable spectrum-averaged reaction cross section, the neutron energy spectrum at the monitor location must be calculated.

The specific activity of each of the monitors is determined using established ASTM procedures.^[7,8,9,10,11] Following sample preparation, the activity of each monitor is determined by means of a lithium-drifted germanium, Ge(Li), gamma spectrometer. The overall standard deviation of the measured data is a function of the precision of sample weighing, the uncertainty in counting, and the acceptable error in detector calibration. For the samples removed from Sequoyah Unit 2, the overall 2σ deviation in the measured data is determined to be plus or minus 10 percent. The neutron energy spectra are determined analytically using the method described in paragraph 6-1.

Having the measured activity of the monitors and the neutron energy spectra at the locations of interest, the calculation of the neutron flux proceeds as follows. The reaction product activity in the monitor is expressed as

$$R = \frac{N_0}{A} f_i \gamma \int_E \sigma(E) \phi(E) dE \sum_{j=1}^n \frac{P_j}{P_{\max}} (1 - e^{-\lambda t_j}) e^{-\lambda t_d} \quad (6-2)$$

where

- R = induced product activity
- N_0 = Avogadro's number
- A = atomic weight of the target isotope
- f_i = weight fraction of the target isotope in the target material
- γ = number of product atoms produced per reaction
- $\sigma(E)$ = energy dependent reaction cross section
- $\phi(E)$ = energy dependent neutron flux at the monitor location with the reactor at full power
- P_j = average core power level during irradiation period j
- P_{\max} = maximum or reference core power level
- λ = decay constant of the product isotope
- t_j = length of irradiation period j
- t_d = decay time following irradiation period j

Because neutron flux distributions are calculated using multigroup transport methods and, further, because the prime interest is in the fast neutron flux above 1.0 MeV, spectrum-averaged reaction cross sections are defined such that the integral term in equation (6-2) is replaced by the following relation.

$$\int_E \sigma(E) \phi(E) dE = \bar{\sigma} \phi (E > 1.0 \text{ MeV})$$

where

$$\bar{\sigma} = \frac{\int_0^{\infty} \sigma(E) \phi(E) dE}{\int_{1.0 \text{ MeV}}^{\infty} \phi(E) dE} = \frac{\sum_{g=1}^N \sigma_g \phi_g}{\sum_{g=g_{1.0 \text{ MeV}}}^N \phi_g}$$

Thus, equation (6-2) is rewritten

$$R = \frac{N_0}{A} f_i y \bar{\sigma} \phi (E > 1.0 \text{ MeV}) \sum_{j=1}^N \frac{P_j}{P_{\max}} (1 - e^{-\lambda t_j}) e^{-\lambda t_d}$$

or, solving for the neutron flux,

$$\phi(E > 1.0 \text{ MeV}) = \frac{R}{\frac{N_0}{A} f_i y \bar{\sigma} \sum_{j=1}^n \frac{P_j}{P_{\max}} (1 - e^{-\lambda t_j}) e^{-\lambda t_d}} \quad (6-3)$$

the total fluence above 1.0 MeV is then given by

$$\Phi(E > 1.0 \text{ MeV}) = \phi(E > 1.0 \text{ MeV}) \sum_{j=1}^n \frac{P_j}{P_{\max}} t_j \quad (6-4)$$

where

$$\sum_{j=1}^n \frac{P_j}{P_{\max}} t_j = \text{total effective full power seconds of reactor operation up to the time of capsule removal}$$

An assessment of the thermal neutron flux levels within the surveillance capsules is obtained from the bare and cadmium-covered $\text{Co}^{59} (n, \gamma) \text{Co}^{60}$ data by means of cadmium ratios and the use of a 37-barn, 2,200 m/sec cross section. Thus,

$$\phi_{\text{Th}} = \frac{R_{\text{bare}} \left[\frac{D-1}{D} \right]}{\frac{N_0}{A} f_i y \bar{\sigma} \sum_{j=1}^n \frac{P_j}{P_{\max}} (1 - e^{-\lambda t_j}) e^{-\lambda t_d}} \quad (6-5)$$

where D is defined as $R_{\text{bare}}/R_{\text{Cd covered}}$.

6-4. TRANSPORT ANALYSIS RESULTS

Results of the S_n transport calculations for the Sequoyah Unit 2 reactor are summarized in Figures 6-3 through 6-8 and in Tables 6-3 through 6-5. In Figure 6-3, the calculated maximum neutron flux levels at the surveillance capsule centerline, pressure vessel inner radius, 1/4 thickness location, and 3/4 thickness location are presented as a function of azimuthal angle. The influence of the surveillance capsules on the fast neutron flux distribution is clearly evident. In Figure 6-4, the radial distribution of maximum fast neutron flux ($E > 1.0$ MeV) through the thickness of the reactor pressure vessel is shown. The relative axial variation of neutron flux within the vessel is given in Figure 6-5. Absolute axial variations of fast neutron flux may be obtained by multiplying the levels given in Figure 6-3 or 6-4 by the appropriate values from Figure 6-5.

In Figure 6-6, the radial variations of fast neutron flux within surveillance capsules at 4 and 40 degrees are presented. These data, in conjunction with the maximum vessel flux, are used to develop lead factors for each of the capsules. Here the lead factor is defined as the ratio of the fast neutron flux ($E > 1.0$ MeV) at the dosimeter block location (capsule center) to the maximum fast neutron flux at the pressure vessel inner radius. Updated lead factors for all of the Sequoyah Unit 2 surveillance capsules are listed in Table 6-3.

Since the neutron flux monitors contained within the surveillance capsules are not all located at the same radial location, the measured disintegration rates are analytically adjusted for the gradients that exist within the capsules so that flux and fluence levels may be derived on a common basis at a common location. This point of comparison was chosen to be the capsule center. Analytically determined reaction rate gradients for use in the adjustment procedures are shown in Figures 6-7 and 6-8 for capsules at 4 and 40 degrees. All of the applicable fast neutron reactions are included.

In order to derive neutron flux and fluence levels from the measured disintegration rates, suitable spectrum-averaged reaction cross sections are required. The neutron energy spectrum calculated to exist at the center of each of the Sequoyah surveillance capsules is listed in Table 6-4. The associated spectrum-averaged cross sections for each of the fast neutron reactions are given in Table 6-5.

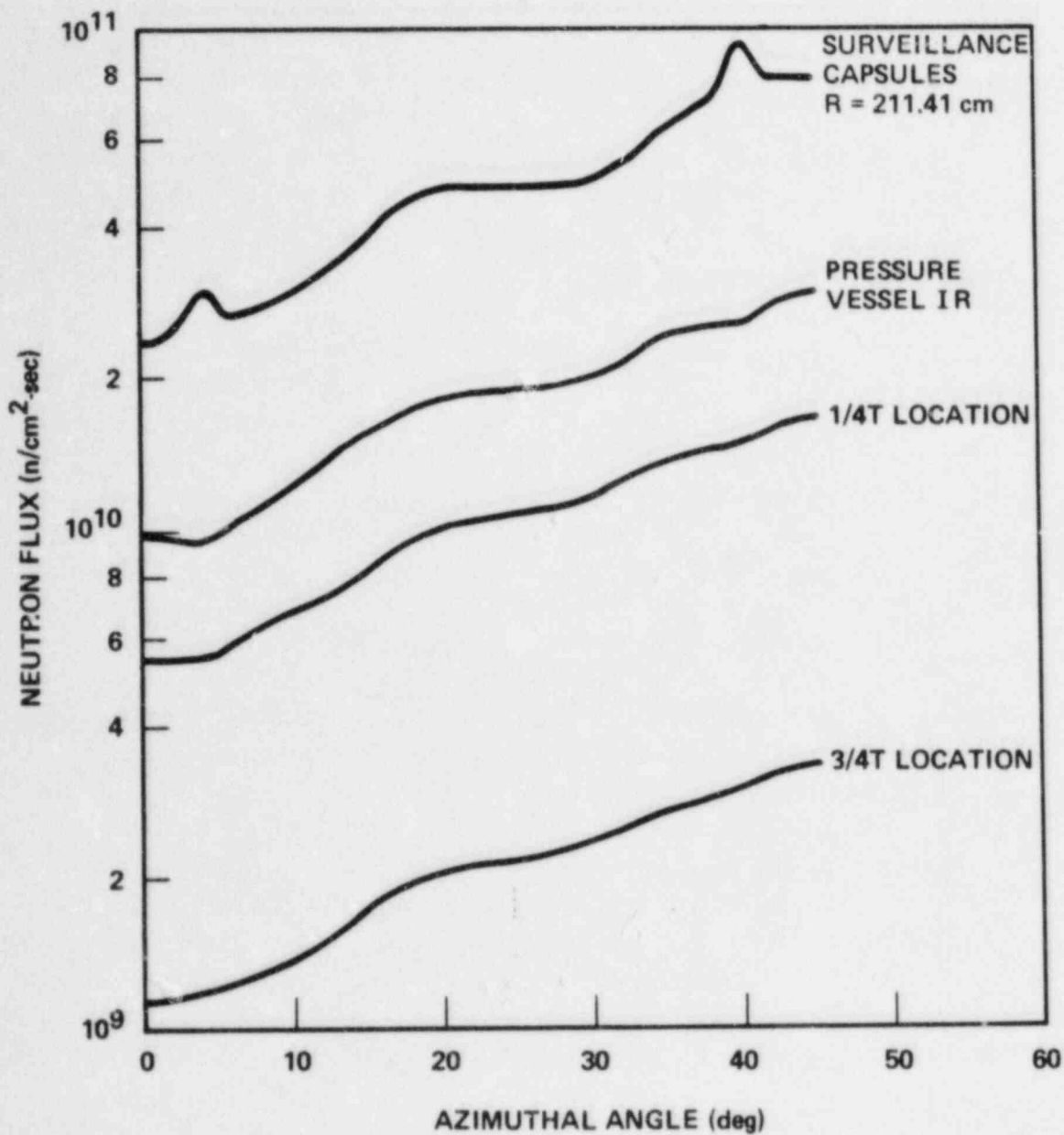


Figure 6-3. Calculated Azimuthal Distribution of Maximum Fast Neutron Flux ($E > 1.0$ MeV) Within the Pressure Vessel — Surveillance Capsule Geometry

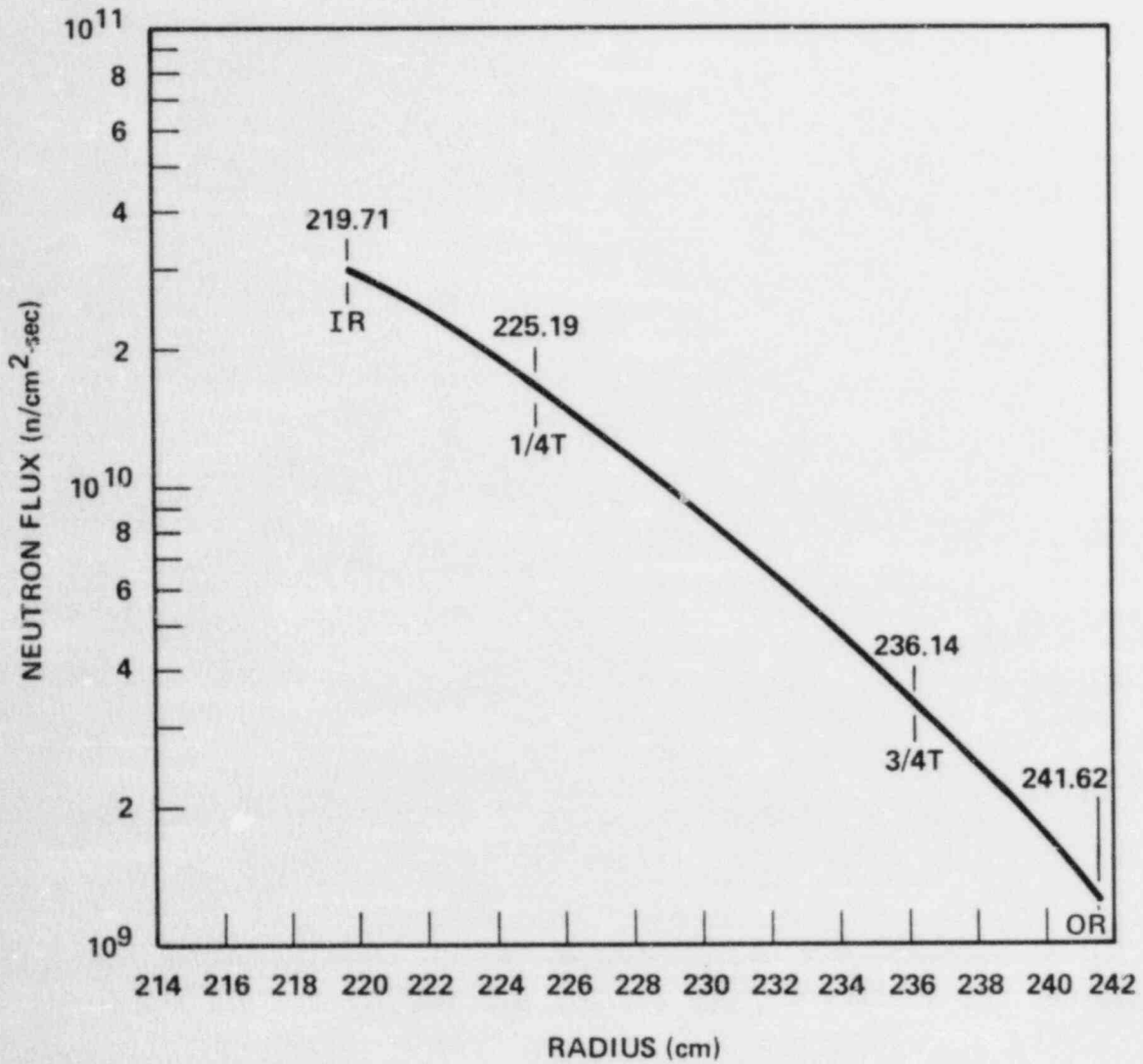


Figure 6-4. Calculated Radial Distribution of Maximum Fast Neutron Flux ($E > 1.0$ MeV) Within the Pressure Vessel

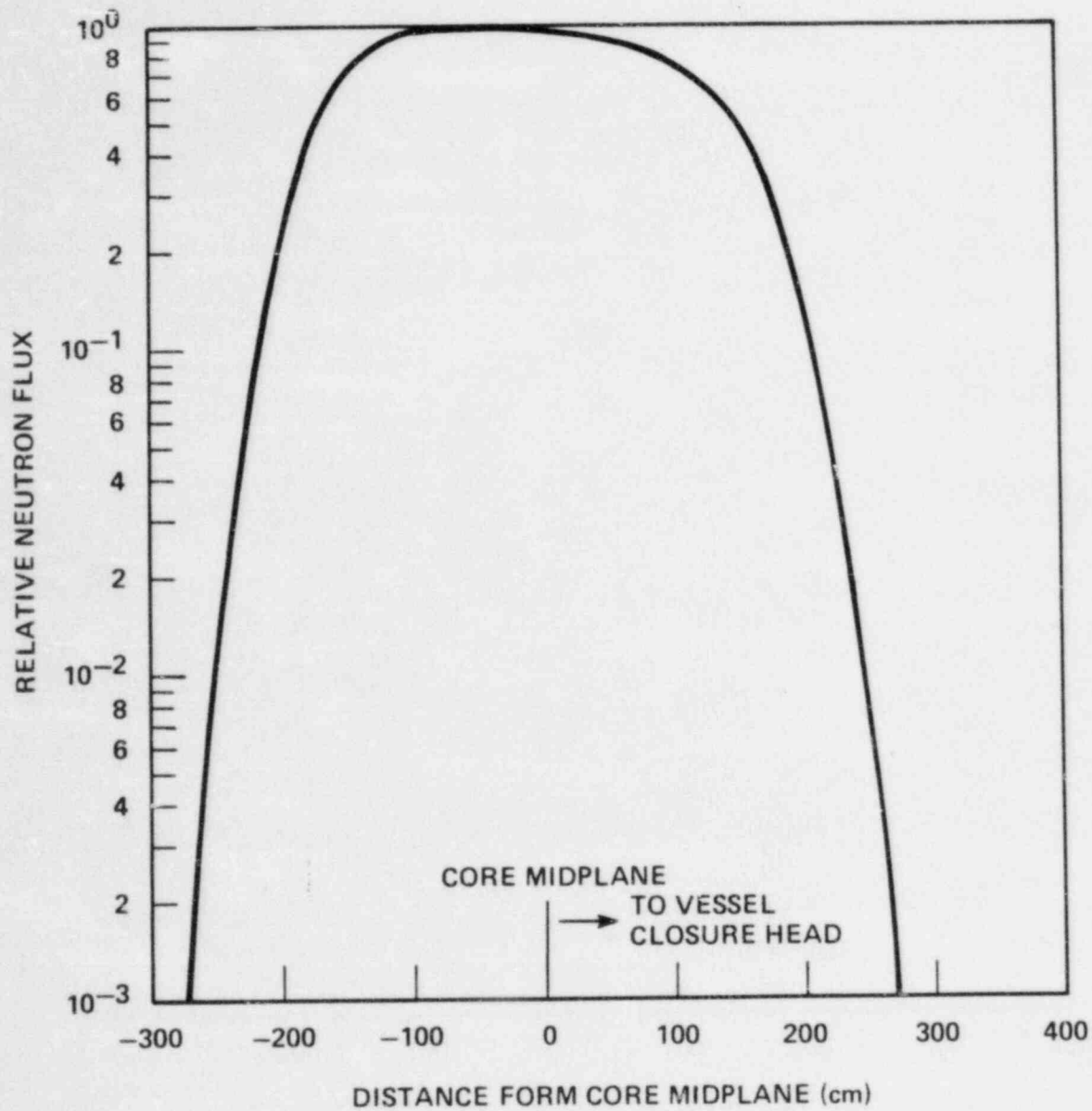


Figure 6-5. Relative Axial Variation of Fast Neutron Flux ($E > 1.0$ MeV) Within the Pressure Vessel

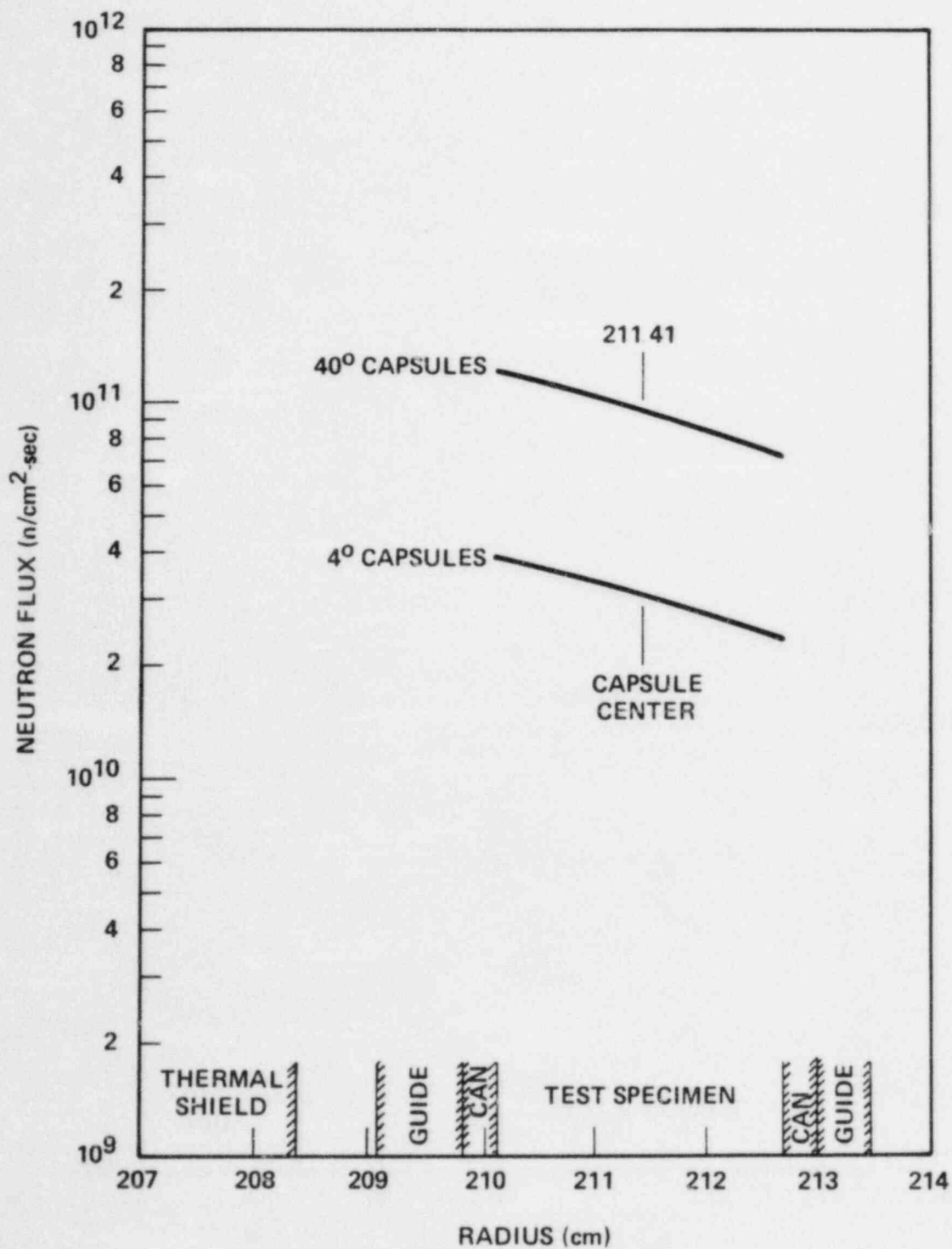


Figure 6-6. Calculated Radial Distribution of Maximum Fast Neutron Flux ($E > 1.0$ MeV) Within the Surveillance Capsule

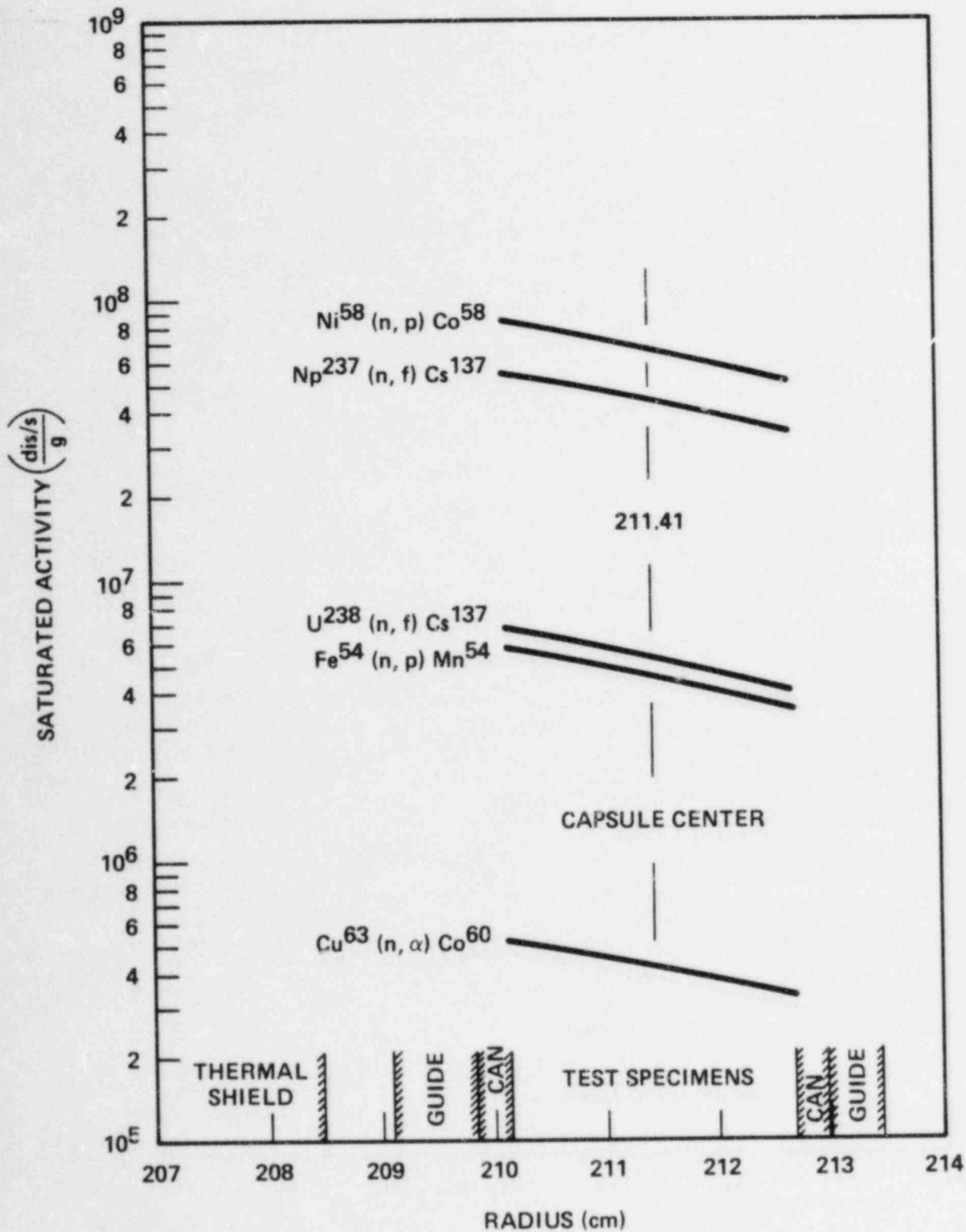


Figure 6-7. Calculated Variation of Fast Neutron Flux Monitor Saturated Activity Within Capsules Located at 40 Degrees

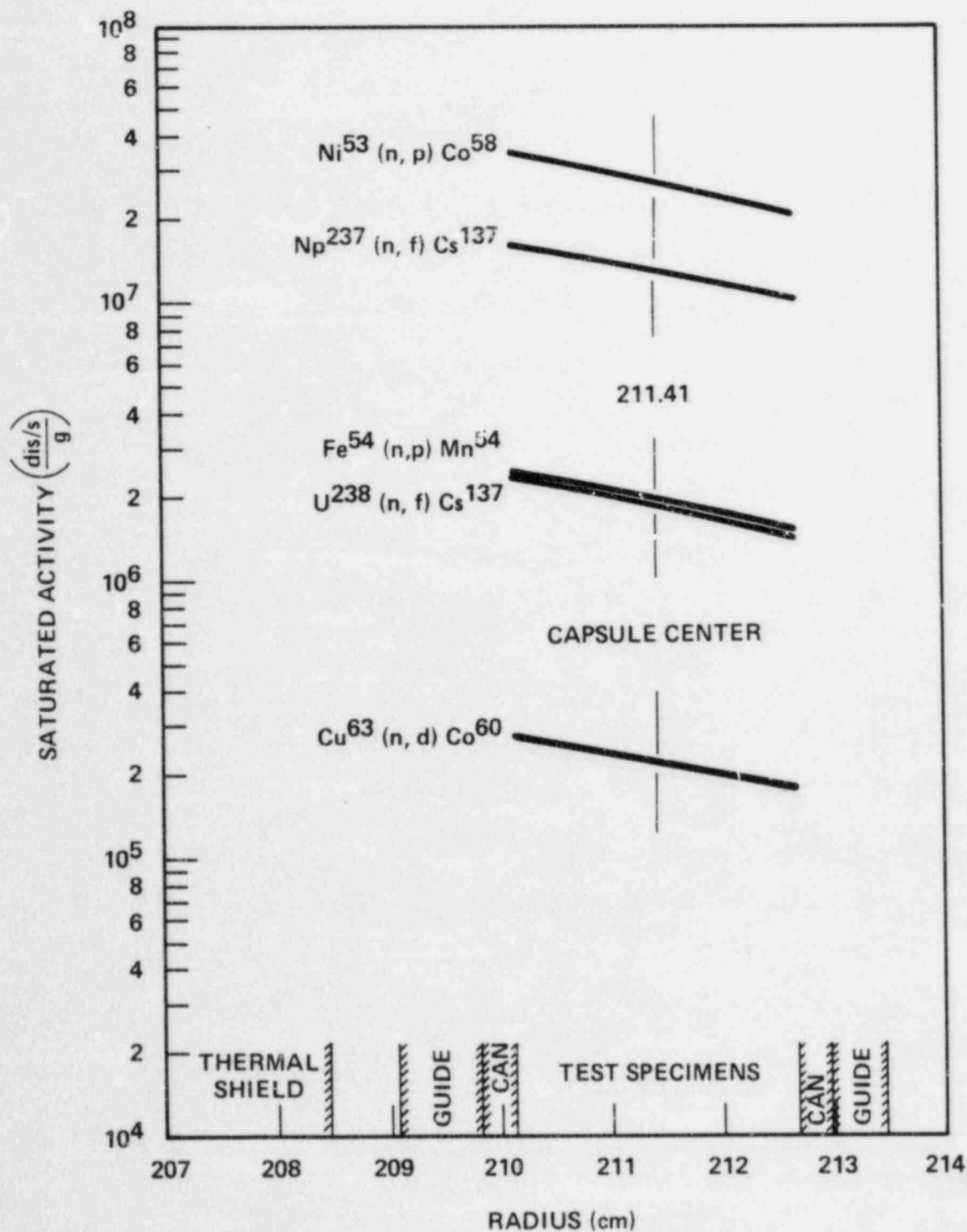


Figure 6-8. Calculated Variation of Fast Neutron Flux Monitor Saturated Activity Within Capsules Located at 4 Degrees

TABLE 6-3

CALCULATED FAST NEUTRON FLUX ($E > 1.0$ MeV) AND LEAD FACTORS FOR SEQUOYAH UNIT 2 SURVEILLANCE CAPSULES

Capsule Identification	Azimuthal Location (deg)	$\phi(E > 1.0 \text{ MeV})$ (n/cm ² -sec)	Lead Factor
S	4	3.04×10^{10}	1.02
V	4	3.04×10^{10}	1.02
W	4	3.04×10^{10}	1.02
Z	4	3.04×10^{10}	1.02
T	40	9.44×10^{10}	3.17
U	40	9.44×10^{10}	3.17
X	40	9.44×10^{10}	3.17
Y	40	9.44×10^{10}	3.17

TABLE 6-4

**CALCULATED NEUTRON ENERGY SPECTRA AT THE CENTER OF
THE SEQUOYAH UNIT 2 SURVEILLANCE CAPSULES**

Group No.	ϕ (n/cm ² -sec)		Group No.	ϕ (n/cm ² -sec)	
	4° Capsules	40° Capsules		4° Capsules	40° Capsules
1	1.35x10 ⁷	2.08x10 ⁷	25	3.59x10 ⁹	3.42x10 ¹⁰
2	4.85x10 ⁷	7.65x10 ⁷	26	8.10x10 ⁹	3.29x10 ¹⁰
3	1.56x10 ⁸	2.67x10 ⁸	27	6.50x10 ⁹	2.67x10 ¹⁰
4	2.74x10 ⁸	4.89x10 ⁸	28	4.80x10 ⁹	1.99x10 ¹⁰
5	4.32x10 ⁸	8.20x10 ⁸	29	1.68x10 ⁹	6.92x10 ⁹
6	9.33x10 ⁸	1.85x10 ⁹	30	1.04x10 ⁹	4.27x10 ⁹
7	1.18x10 ⁹	2.57x10 ⁹	31	1.71x10 ⁹	7.15x10 ⁹
8	2.07x10 ⁹	5.17x10 ⁹	32	1.05x10 ⁹	4.41x10 ⁹
9	1.62x10 ⁹	4.54x10 ⁹	33	2.52x10 ⁹	1.05x10 ¹⁰
10	1.27x10 ⁹	3.71x10 ⁹	34	4.21x10 ⁹	1.75x10 ¹⁰
11	1.46x10 ⁹	4.38x10 ⁹	35	5.66x10 ⁹	2.35x10 ¹⁰
12	7.19x10 ⁸	2.19x10 ⁹	36	5.16x10 ⁹	2.17x10 ¹⁰
13	2.12x10 ⁸	6.52x10 ⁸	37	7.79x10 ⁹	3.31x10 ¹⁰
14	1.04x10 ⁹	3.22x10 ⁹	38	4.42x10 ⁹	1.88x10 ¹⁰
15	2.67x10 ⁹	8.37x10 ⁹	39	4.68x10 ⁹	2.01x10 ¹⁰
16	3.21x10 ⁹	1.05x10 ¹⁰	40	6.27x10 ⁹	2.71x10 ¹⁰
17	4.67x10 ⁹	1.57x10 ¹⁰	41	7.59x10 ⁹	3.31x10 ¹⁰
18	8.45x10 ⁹	2.98x10 ¹⁰	42	4.33x10 ⁹	1.90x10 ¹⁰
19	5.73x10 ⁹	2.09x10 ¹⁰	43	5.24x10 ⁹	2.31x10 ¹⁰
20	2.83x10 ⁹	1.04x10 ¹⁰	44	3.46x10 ⁹	1.53x10 ¹⁰
21	8.14x10 ⁹	3.14x10 ¹⁰	45	2.93x10 ⁹	1.29x10 ¹⁰
22	6.21x10 ⁹	2.45x10 ¹⁰	46	5.59x10 ⁹	2.41x10 ¹⁰
23	7.46x10 ⁹	2.93x10 ¹⁰	47	1.41x10 ¹⁰	5.66x10 ¹⁰
24	6.51x10 ⁹	2.59x10 ¹⁰			

TABLE 6-5

SPECTRUM-AVERAGED REACTION CROSS SECTIONS AT THE
CENTER OF SEQUOYAH UNIT 2 SURVEILLANCE CAPSULES

Reaction	$\bar{\sigma}$ (barns) ^[a]	
	Capsules at 4°	Capsules at 40°
Fe ⁵⁴ (n,p) Mn ⁵⁴	0.0980	0.0735
Cu ⁶³ (n, α) Co ⁶⁰	0.00112	0.000659
Ni ⁵⁸ (n,p) Co ⁵⁸	0.127	0.0993
Np ²³⁷ (n,f) Cs ¹³⁷	2.62	2.83
U ²³⁸ (n,f) Cs ¹³⁷	0.385	0.385

$$[a] \bar{\sigma} = \frac{\int_0^{\infty} \sigma(E)\phi(E)dE}{\int_{1 \text{ MeV}}^{\infty} \phi(E)dE}$$

6-5. DOSIMETRY RESULTS

The irradiation history of the Sequoyah Unit 2 reactor up to the time of removal of Capsule T is listed in Table 6-6. Comparisons of measured and calculated saturated activity of the flux monitors contained in Capsule T based on the irradiation history shown in Table 6-6 are given in Table 6-7. The data are presented as measured at the actual monitor locations as well as adjusted to the capsule center. All gradient adjustments to the capsule center were based on the data presented in Figure 6-7.

The fast neutron ($E > 1.0$ MeV) flux and fluence levels derived for Capsule T are presented in Table 6-8. The thermal neutron flux obtained from the cobalt-aluminum monitors is summarized in Table 6-9. Due to the relatively low thermal neutron flux at the capsule location, no burnup correction was made to any of the measured activities. The maximum error introduced by this assumption is estimated to be less than 1 percent for the $\text{Ni}^{58}(n,p)\text{Co}^{58}$ reaction and even less significant for all of the other fast neutron reactions.

An examination of Table 6-8 shows that the fast neutron flux ($E > 1.0$ MeV) derived from the five threshold reactions ranges from 6.69×10^{10} to 8.46×10^{10} n/cm²-sec, a total span of less than 10 percent. It may also be noted that the calculated flux value of 9.44×10^{10} n/cm²-sec exceeds all of the measured values, with calculation to experimental ratios ranging from 1.12 to 1.41.

Comparisons of measured and calculated current fast neutron exposures for Capsule T as well as for the inner radius of the pressure vessel are presented in Table 6-10. Measured values are given based on the $\text{Fe}^{54}(n,p)\text{Mn}^{54}$ reaction alone as well as for the average of all five threshold reactions. Based on the data given in Table 6-10, the best estimate exposure of Capsule T is

$$\Phi_T = 2.20 \times 10^{18} \text{ n/cm}^2 (E > 1 \text{ MeV})$$

Since the calculated fluence levels were based on conservative representations of core power distributions derived for long-term operation while the Capsule T data are representative only of cycle 1 operation, it is recommended that projections of vessel toughness into the future be based on design basis calculated fluence levels. Withdrawal of future surveillance capsules should further substantiate the adequacy of this approach.

TABLE 6-6

**IRRADIATION HISTORY OF SEQUOYAH UNIT 2
SURVEILLANCE CAPSULE T**

Month	Year	P _j (MW)	P _{max} (MW)	P _j /P _{max}	Irradiation Time (Days)	Decay Time ^(a) (Days)
12	1981	27	3565	.007	9	679
1	1982	264	3565	.074	31	648
2	1982	763	3565	.214	28	620
3	1982	1223	3565	.343	31	589
4	1982	2251	3565	.632	30	559
5	1982	1282	3565	.360	31	528
6	1982	2706	3565	.759	30	498
7	1982	3389	3565	.951	31	467
8	1982	3287	3565	.922	31	436
9	1982	2883	3565	.809	30	406
10	1982	3123	3565	.876	31	375
11	1982	1366	3565	.383	30	345
12	1982	4	3565	.001	31	314
1	1983	3054	3565	.857	31	283
2	1983	3495	3565	.980	28	255
3	1983	3403	3565	.955	31	224
4	1983	3472	3565	.974	30	194
5	1983	3485	3565	.978	31	163
6	1983	3160	3565	.886	30	133
7	1983	3179	3565	.892	19	114

EFPS = 3.28E + 07 SEC
= 1.04 EFPY

[a] Decay time is referenced to 11/11/83.

TABLE 6-7

**COMPARISON OF MEASURED AND CALCULATED FAST NEUTRON FLUX
MONITOR SATURATED ACTIVITIES FOR CAPSULE T**

Reaction and Axial Position	Radial Location (cm)	Saturated Activity		Adjusted Saturated Activity	
		$\left(\frac{\text{dis/s}}{\text{g}}\right)$		$\left(\frac{\text{dis/s}}{\text{g}}\right)$	
		Capsule T	Calculated	Capsule T	Calculated
<u>Fe⁵⁴ (n,p) Mn⁵⁴</u>					
Top	211.68	3.01x10 ⁶		3.17x10 ⁶	
Top-Middle	211.68	3.03x10 ⁶		3.20x10 ⁶	
Middle	211.68	3.01x10 ⁶		3.17x10 ⁶	
Bottom-Middle	211.68	3.08x10 ⁶		3.25x10 ⁶	
Bottom	211.68	3.11x10 ⁶		3.28x10 ⁶	
Average		3.05x10 ⁶	4.30x10 ⁶	3.21x10 ⁶	4.53x10 ⁶
<u>Cu⁶³ (n,a) Co⁶⁰</u>					
Top-Middle	211.18	3.22x10 ⁵		3.06x10 ⁵	
Middle	211.18	3.24x10 ⁵		3.08x10 ⁵	
Bottom-Middle	211.18	3.36x10 ⁵		3.20x10 ⁵	
Average		3.27x10 ⁵	4.32x10 ⁵	3.11x10 ⁵	4.11x10 ⁵
<u>Ni⁵⁸ (n,p) Co⁵⁸</u>					
Top-Middle	212.18	4.06x10 ⁷		4.66x10 ⁷	
Middle	212.18	3.99x10 ⁷		4.58x10 ⁷	
Bottom-Middle	212.18	4.16x10 ⁷		4.78x10 ⁷	
Average		4.07x10 ⁷	5.75x10 ⁷	4.67x10 ⁷	6.59x10 ⁷
<u>NP²³⁷ (n,f) Cs¹³⁷</u>					
Middle	211.41	3.95x10 ⁷	4.41x10 ⁷	3.95x10 ⁷	4.41x10 ⁷
<u>U²³⁸ (n,f) Cs¹³⁷</u>					
Middle	211.41	5.02x10 ⁶	5.31x10 ⁶	5.02x10 ⁶	5.31x10 ⁶

TABLE 6-8

RESULTS OF FAST NEUTRON DOSIMETRY FOR CAPSULE T

Reaction	$\frac{\text{dis/s}}{\text{g}}$		$\phi (E > 1.0 \text{ Mev})$ (n/cm ² -sec)		$\phi (E > 1.0 \text{ Mev})$ (n/cm ²)	
	Measured	Calculated	Measured	Calculated	Measured	Calculated
Fe ⁵⁴ (n,p)Mn ⁵⁴	3.21x10 ⁶	4.53x10 ⁷	6.70x10 ¹⁰	9.44x10 ¹⁰	2.20x10 ¹⁸	3.10x10 ¹⁸
Cu ⁶³ (n, α)Co ⁶⁰	3.11x10 ⁵	4.11x10 ⁵	7.14x10 ¹⁰	9.44x10 ¹⁰	2.34x10 ¹⁸	3.10x10 ¹⁸
Ni ⁵⁸ (n,p)Co ⁵⁸	4.67x10 ⁷	6.59x10 ⁷	6.69x10 ¹⁰	9.44x10 ¹⁰	2.19x10 ¹⁸	3.10x10 ¹⁸
Np ²³⁷ (n,f)Cs ¹³⁷	3.95x10 ⁷	4.41x10 ⁷	8.46x10 ¹⁰	9.44x10 ¹⁰	2.77x10 ¹⁸	3.10x10 ¹⁸
U ²³⁸ (n,f)Cs ¹³⁷ [a]	4.42x10 ⁶	5.31x10 ⁶	7.19x10 ¹⁰	9.44x10 ¹⁰	2.36x10 ¹⁸	3.10x10 ¹⁸

[a] U²³⁸ adjusted saturated activity has been multiplied by 0.88 to correct for 350 ppm U²³⁵ impurity.

TABLE 6-9

RESULTS OF THERMAL NEUTRON DOSIMETRY FOR CAPSULE T

Axial Location	Saturated Activity ($\frac{\text{dis/s}}{\text{g}}$)		ϕ_{Th} ($\text{n/cm}^2\text{-sec}$)
	Bare	Cd-Covered	
Top	7.01×10^7	2.79×10^7	7.48×10^{10}
Bottom	6.94×10^7	2.73×10^7	7.38×10^{10}
Average	6.98×10^7	2.76×10^7	7.43×10^{10}

TABLE 6-10

SUMMARY OF NEUTRON DOSIMETRY RESULTS FOR CAPSULE T

Location	Current ϕ ($E > 1.0$ mev) (n/cm^2)		EOL ϕ ($E > 1.0$ mev) (n/cm^2)	
	Measured	Calculated	Measured	Calculated
Capsule T	2.20×10^{18}	3.10×10^{18}		
Vessel IR	6.94×10^{17}	9.78×10^{17}	2.13×10^{19}	3.01×10^{19}
Vessel 1/4T	3.85×10^{17}	5.42×10^{17}	1.18×10^{19}	1.67×10^{19}
Vessel 3/4T	7.93×10^{16}	1.12×10^{16}	2.44×10^{18}	3.43×10^{18}

Note: EOL fluences are based on operation at 3565 MWt for effective full-power years.

SECTION 7

SURVEILLANCE CAPSULE REMOVAL SCHEDULE

The following removal schedule per ASTM E185-82 is recommended for future capsules to be removed from the Sequoyah Unit 2 reactor vessel:

Capsule	Vessel Location (deg)	Lead Factor	Removal Time ^[a]	Estimated Fluence (n/cm ²)
T	40	3.17	1.04 (removed)	2.20 x 10 ¹⁸
U	140	3.17	3	8.39 x 10 ¹⁸
X	220	3.17	6	1.68 x 10 ¹⁹ [b]
Y	320	3.17	11	3.06 x 10 ¹⁹ [c]
S	4	1.02	34	3.06 x 10 ¹⁹
V	176	1.02	standby	
W	184	1.02	standby	
Z	356	1.02	standby	

[a] Effective full power years from plant startup

[b] Approximate fluence at 1/4 thickness vessel wall at end of life

[c] Approximate fluence at vessel inner wall at end of life

SECTION 8

REFERENCES

1. Yanichko, S. E., Davidson, J. A., and Phillips, J. H., "Tennessee Valley Authority Sequoyah Unit No. 2 Reactor Vessel Radiation Surveillance Program," WCAP-8513, November, 1975.
2. ASTM Standard E185-73, "Recommended Practice for Surveillance Tests for Nuclear Reactors" in ASTM Standards, Part 45 (1973), American Society for Testing and Materials, Philadelphia, Pa., 1973.
3. Regulatory Guide 1.99, Revision 1, "Effects of Residual Elements on Predicted Radiation Damage to Reactor Vessel Materials," U.S. Nuclear Regulatory Commission, April 1977.
4. Soltesz, R. G., Disney, R. K., Jedruch, J., and Ziegler, S. L., "Nuclear Rocket Shielding Methods, Modification, Updating and Input Data Preparation. Vol. 5 — Two-Dimensional Discrete Ordinates Transport Technique," WANL-PR(LL)034, Vol. 5, August 1970.
5. SAILOR RSIC Data Library Collection DLC-76, Coupled Self-Shielded, 47 Neutron, 20 Gamma-Ray, P3, Cross Section Library for Light Water Reactors.
6. Benchmark Testing of Westinghouse Neutron Transport Analysis Methodology (To be published).
7. ASTM Designation 261-77, "Standard Practice for Measuring Neutron Flux, Fluence, and Spectra by Radioactivation Techniques," in ASTM Standards (1981), Part 45, Nuclear Standards, pp 915-926, American Society for Testing and Materials, Philadelphia, Pa., 1981.
8. ASTM Designation 262-77, "Standard Method for Measuring Thermal Neutron Flux by Radioactivation Techniques," in ASTM Standards (1981), Part 45, Nuclear Standards, pp 927-935, American Society for Testing and Materials, Philadelphia, Pa., 1981.

9. ASTM Designation 263-77, "Standard Method for Measuring Fast-Neutron Flux by Radioactivation of Iron," in ASTM Standards (1981), Part 45, Nuclear Standards, pp 936-941, American Society for Testing and Materials, Philadelphia, Pa., 1981.
10. ASTM Designation 481-78, "Standard Method of Measuring Neutron-Flux Density by Radioactivation of Cobalt and Silver," in ASTM Standards (1981), Part 45, Nuclear Standards, pp 1063-1070, American Society for Testing and Materials, Philadelphia, Pa., 1981.
11. ASTM Designation 264-77, "Standard Method for Measuring Fast-Neutron Flux by Radioactivation of Nickel," in ASTM Standards (1981), Part 45, Nuclear Standards, pp 942-945, American Society for Testing and Materials, Philadelphia, Pa., 1981.

APPENDIX A

HEATUP AND COOLDOWN LIMIT CURVES FOR NORMAL OPERATION

A-1. INTRODUCTION

Heatup and cooldown limit curves are calculated using the most limiting value of RT_{NDT} (reference nil-ductility temperature). The most limiting RT_{NDT} of the material in the core region of the reactor vessel is determined by using the preservice reactor vessel material properties and estimating the radiation-induced ΔRT_{NDT} . RT_{NDT} is designated as the higher of either the drop weight nil-ductility transition temperature (NDTT) or the temperature at which the material exhibits at least 50 ft-lb of impact energy and 35-mil lateral expansion (normal to the major working direction) minus 60°F.

RT_{NDT} increases as the material is exposed to fast-neutron radiation. Thus, to find the most limiting RT_{NDT} at any time period in the reactor's life, ΔRT_{NDT} due to the radiation exposure associated with that time period must be added to the original unirradiated RT_{NDT} . The extent of the shift in RT_{NDT} is enhanced by certain chemical elements (such as copper and phosphorus) present in reactor vessel steels. Design curves which show the effect of fluence and copper and phosphorus contents on ΔRT_{NDT} for reactor vessel steels are shown in Figure A-1.

Given the copper content of the most limiting material, the radiation-induced ΔRT_{NDT} can be estimated from Figure A-1. Fast neutron fluence ($E > 1$ Mev) at the vessel inner surface, the 1/4 T (wall thickness), and 3/4 T (wall thickness) vessel locations are given as a function of full-power service life in Figure A-2. The data for all other ferritic materials in the reactor coolant pressure boundary are examined to insure that no other component will be limiting with respect to RT_{NDT} .

A-2. FRACTURE TOUGHNESS PROPERTIES

The preirradiation fracture-toughness properties of the Sequoyah Unit 2 reactor vessel materials are presented in Table A-1. The fracture-toughness properties of the ferritic material in the reactor coolant pressure boundary are determined in accordance with the NRC Regulatory Standard Review Plan.⁽¹⁾ The postirradiation fracture-toughness properties of the reactor vessel beltline material were obtained directly from the Sequoyah Unit 2 Vessel Material Surveillance Program.

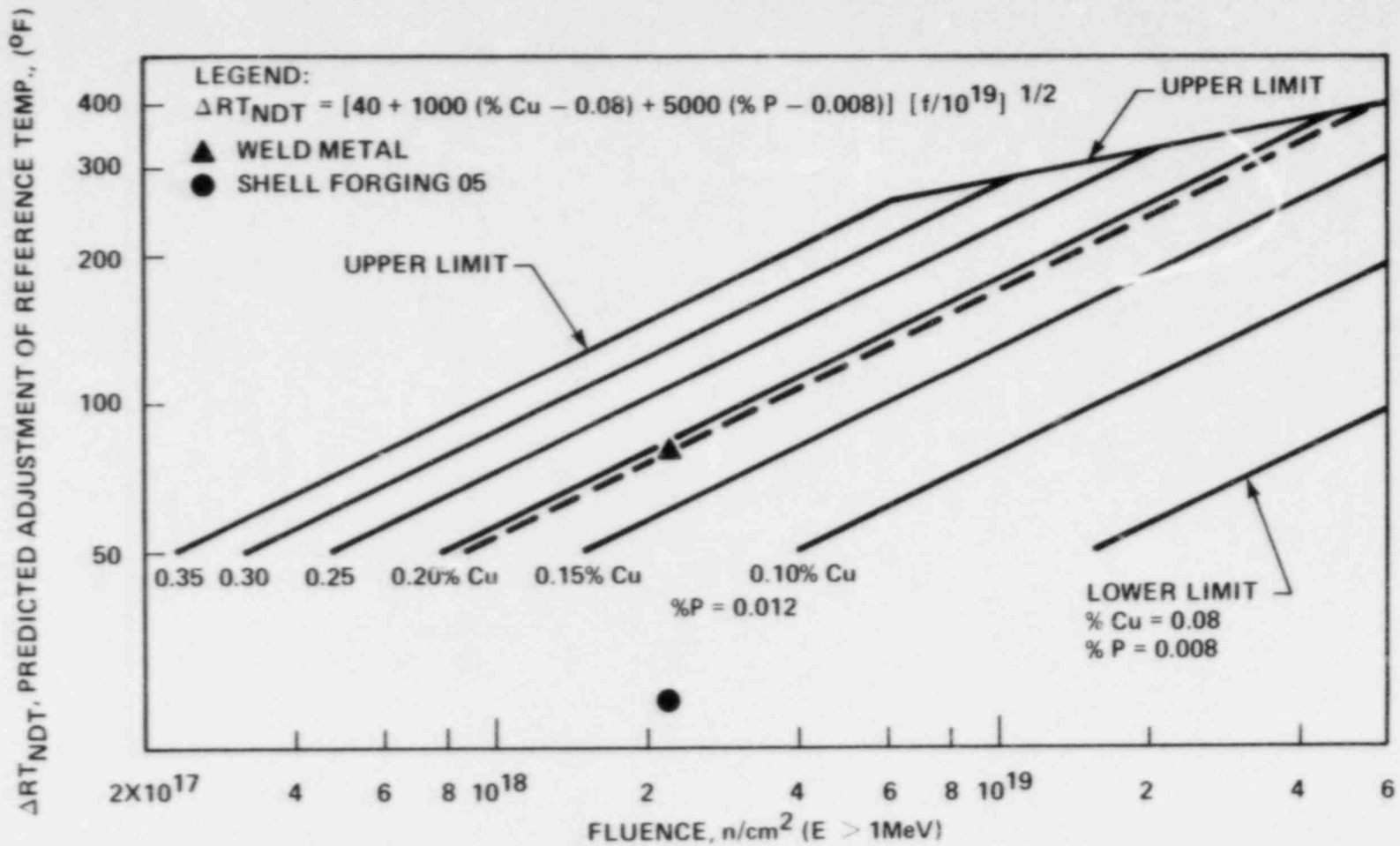


Figure A-1. Predicted Adjustment of Reference Temperature, ΔRT_{NDT} , as a Function of Fluence and Copper Content. For Copper and Phosphorus Contents Other Than Those Plotted, Use the Expression for ΔRT_{NDT} Given on the Figure.

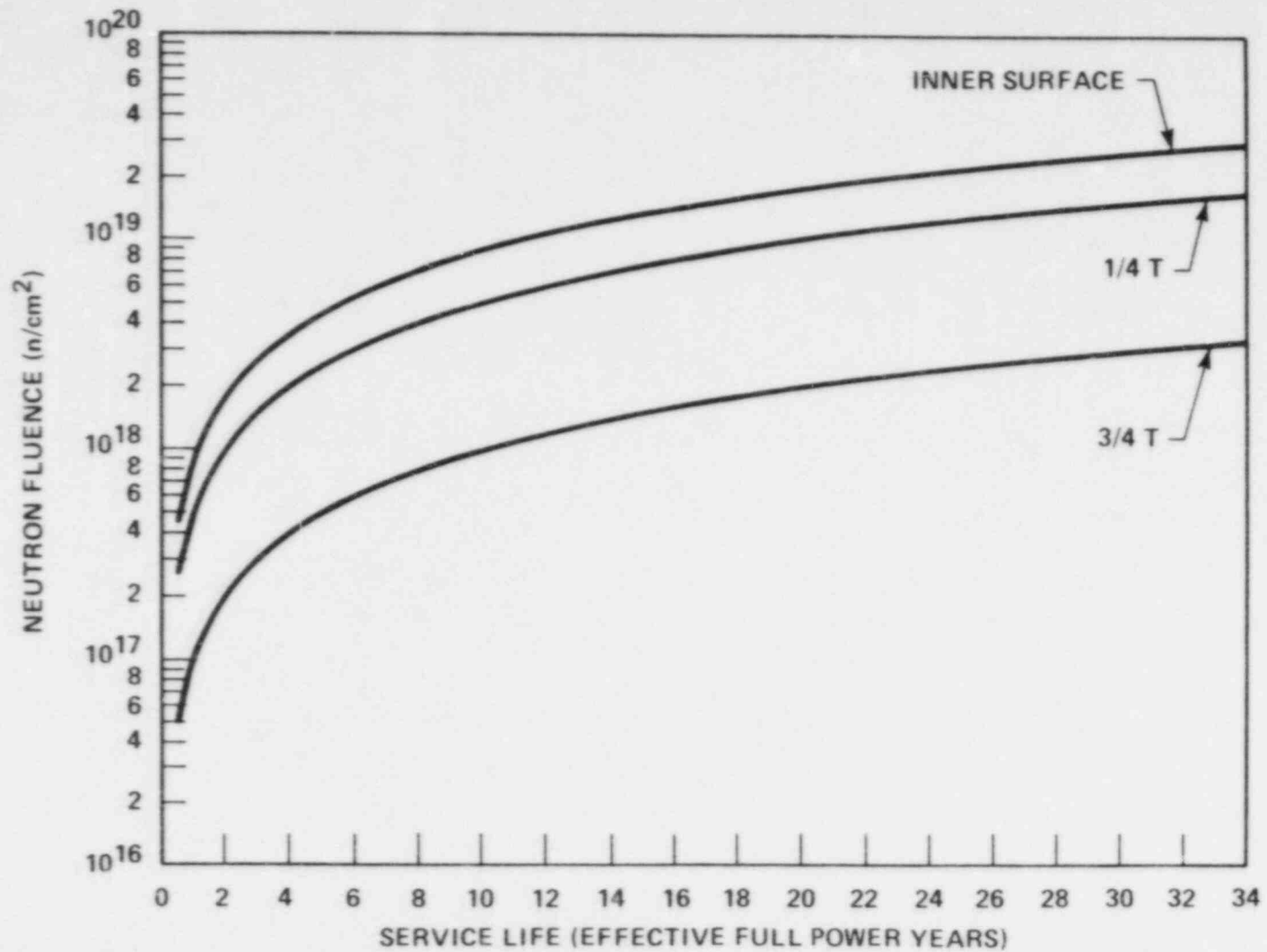


Figure A-2. Fast Neutron Fluence ($E > 1$ MeV) as a Function of Full Power Service Life

TABLE A-1

SEQUOYAH UNIT 2 REACTOR VESSEL TOUGHNESS DATA

Component	Heat No.	Material Grade	CU (%)	P (%)	NDTT (°F)	Minimum 50 ft-lb/35 MIL TEMP (°F)		RT _{NDT} (°F)	Average Upper Shelf (FT-LB)	
						PMWD ^(a)	NMWD ^(b)		PMWD ^(a)	NMWD ^(b)
CL Hd. Dome	52899-1	A533BCL1	—	—	-13	28	48 ^(c)	-12	75 ^(d)	
CL Hd. Ring	—	A508CL2	—	—	5	34	54 ^(c)	5	1255 ^(d)	
Hd Flange	4890	A508CL2	—	—	-13	< -67	< -67 ^(c)	-13	141 ^(d)	
Vessel Flange	4832	A508CL2	—	—	-22	-47	-27 ^(c)	-22	155.5 ^(d)	
Inlet Nozzle	4868	A508CL2	—	—	-22	41	61 ^(c)	1	79 ^(d)	
Inlet Nozzle	4872	A508CL2	—	—	-22	12	32 ^(c)	-22	108 ^(d)	
Inlet Nozzle	4877	A508CL2	—	—	-31	1	21 ^(c)	-31	113 ^(d)	
Inlet Nozzle	4886	A508CL2	—	—	-31	-52	-32 ^(c)	-31	138 ^(d)	
Outlet Nozzle	4867	A508CL2	—	—	-31	19	39 ^(c)	-21	85 ^(d)	
Outlet Nozzle	4873	A508CL2	—	—	-22	21	41 ^(c)	-19	76 ^(d)	
Outlet Nozzle	4878	A508CL2	—	—	-40	-6	14 ^(c)	-40	105 ^(d)	
Outlet Nozzle	4887	A508CL2	—	—	-22	-11	9 ^(c)	-22	143.5 ^(d)	
Upper Shell	4885	A508CL2	—	—	5	25	45 ^(c)	5	104 ^(d)	
Inter Shell	4853	A508CL2	0.13	.014	-22	19	70	10	138	93
Lower Shell	4994	A508CL2	0.14	.012	-40	8	38	-22	140.5	100
Trans. Ring	4879	A508CL2	—	—	5	27	47 ^(c)	5	98 ^(d)	
Bot. Hd. Ring	52835-1B	A533BCL1	—	—	-4	48	68 ^(c)	8	81 ^(d)	
Bot. Hd. Ring	52835-2	A533BCL1	—	—	-22	25	45 ^(c)	-15	81 ^(d)	
Bot. Hd. Ring	52899-2	A533BCL1	—	—	-13	39	59 ^(c)	-1	62 ^(d)	
Bot. Hd.	52979-1	A533BCL1	—	—	-31	14	34 ^(c)	-26	99.5 ^(d)	
Weld	—	Weld	0.13	.016	-4	—	14	-4	—	101
HAZ	—	HAZ	—	—	-13	—	17	-13	—	120

[a] Parallel to major working direction

[b] Normal to major working direction

[c] Estimate based on the NRC Regulatory Standard Review Plan, Section 5.3.2 MTEB 5-2

[d] Percentage shear not reported, therefore value may not be on the upper shelf

A-3. CRITERIA FOR ALLOWABLE PRESSURE-TEMPERATURE RELATIONSHIPS

The ASME approach for calculating the allowable limit curves for various heatup and cooldown rates specifies that the total stress intensity factor, K_I , for the combined thermal and pressure stresses at any time during heatup or cooldown cannot be greater than the reference stress intensity factor, K_{IR} , for the metal temperature at that time. K_{IR} is obtained from the reference fracture toughness curve, defined in Appendix G to the ASME Code.^[2] The K_{IR} curve is given by the equation:

$$K_{IR} = 26.78 + 1.223 \exp [0.0145 (T - RT_{NDT} + 160)] \quad (A-1)$$

where K_{IR} is the reference stress intensity factor as a function of the metal temperature T and the metal reference nil-ductility temperature RT_{NDT} . Thus, the governing equation for the heatup-cooldown analysis is defined in Appendix G of the ASME Code^[2] as follows:

$$C K_{IM} + K_{It} \leq K_{IR} \quad (A-2)$$

where

K_{IM} is the stress intensity factor caused by membrane (pressure) stress

K_{It} is the stress intensity factor caused by the thermal gradients

K_{IR} is a function of temperature relative to the RT_{NDT} of the material

$C = 2.0$ for Level A and Level B service limits

$C = 1.5$ for hydrostatic and leak test conditions during which the reactor core is not critical

At any time during the heatup or cooldown transient, K_{IR} is determined by the metal temperature at the tip of the postulated flaw, the appropriate value for RT_{NDT} , and the reference fracture toughness curve. The thermal stresses resulting from temperature gradients through the vessel wall are calculated and then the corresponding (thermal) stress intensity factors, K_{It} , for the reference flaw are computed. From Equation (A-2), the pressure stress intensity factors are obtained and, from these, the allowable pressures are calculated.

For the calculation of the allowable pressure-versus-coolant temperature during cooldown, the Code reference flaw is assumed to exist at the inside of the vessel wall. During cooldown, the controlling location of the flaw is always at the inside of the wall because

the thermal gradients produce tensile stresses at the inside, which increase with increasing cooldown rates. Allowable pressure-temperature relations are generated for both steady-state and finite cooldown rate situations. From these relations, composite limit curves are constructed for each cooldown rate of interest.

The use of the composite curve in the cooldown analysis is necessary because control of the cooldown procedure is based on measurement of reactor coolant temperature, whereas the limiting pressure is actually dependent on the material temperature at the tip of the assumed flaw.

During cooldown, the 1/4 T vessel location is at a higher temperature than the fluid adjacent to the vessel ID. This condition, of course, is not true for the steady-state situation. It follows that, at any given reactor coolant temperature, the ΔT developed during cooldown results in a higher value of $K_{I\bar{R}}$ at the 1/4 T location for finite cooldown rates than for steady-state operation. Furthermore, if conditions exist such that the increase in $K_{I\bar{R}}$ exceeds $K_{I\bar{T}}$, the calculated allowable pressure during cooldown will be greater than the steady-state value.

The above procedures are needed because there is no direct control on temperature at the 1/4 T location and, therefore, allowable pressures may unknowingly be violated if the rate of cooling is decreased at various intervals along a cooldown ramp. The use of the composite curve eliminates this problem and insures conservative operation of the system for the entire cooldown period.

Three separate calculations are required to determine the limit curves for finite heatup rates. As is done in the cooldown analysis, allowable pressure-temperature relationships are developed for steady-state conditions as well as finite heatup rate conditions assuming the presence of a 1/4 T defect at the inside of the vessel wall. The thermal gradients during heatup produce compressive stresses at the inside of the wall that alleviate the tensile stresses produced by internal pressure. The metal temperature at the crack tip lags the coolant temperature; therefore, the $K_{I\bar{R}}$ for the 1/4 T crack during heatup is lower than the $K_{I\bar{R}}$ for the 1/4 T crack during steady-state conditions at the same coolant temperature. During heatup, especially at the end of the transient, conditions may exist such that the effects of compressive thermal stresses and lower $K_{I\bar{R}}'s$ do not offset each other, and the pressure-temperature curve based on steady-state conditions no longer represents a lower bound of all similar curves for finite heatup rates when the 1/4 T flaw is considered. Therefore, both cases have to be analyzed in order to insure that at any coolant temperature the lower value of the allowable pressure calculated for steady-state and finite heatup rates is obtained.

The second portion of the heatup analysis concerns the calculation of pressure-temperature limitations for the case in which a 1/4 T deep outside surface flaw is assumed. Unlike the situation at the vessel inside surface, the thermal gradients established at the outside surface during heatup produce stresses which are tensile in nature and thus tend to reinforce any pressure stresses present. These thermal stresses are dependent on both the rate of heatup and the time (or coolant temperature) along the heatup ramp. Since the thermal stresses at the outside are tensile and increase with increasing heatup rates, each heatup rate must be analyzed on an individual basis.

Following the generation of pressure-temperature curves for both the steady-state and finite heatup rate situations, the final limit curves are produced as follows: A composite curve is constructed based on a point-by-point comparison of the steady-state and finite heatup rate data. At any given temperature, the allowable pressure is taken to be the lesser of the three values taken from the curves under consideration. The use of the composite curve is necessary to set conservative heatup limitations because it is possible for conditions to exist wherein, over the course of the heatup ramp, the controlling condition switches from the inside to the outside and the pressure limit must at all times be based on analysis of the most critical criterion. Then, composite curves for the heatup rate data and the cooldown rate data are adjusted for possible errors in the pressure and temperature sensing instruments by the values indicated on the respective curves.

A-4. HEATUP AND COOLDOWN LIMIT CURVES

Limit curves for normal heatup and cooldown of the primary Reactor Coolant System have been calculated using the methods discussed in Section A-3. The derivation of the limit curves is presented in the NRC Regulatory Standard Review Plan.⁽³⁾

Transition temperature shifts occurring in the pressure vessel materials due to radiation exposure have been obtained directly from the reactor pressure vessel surveillance program. Charpy test specimens from Capsule T indicate that the core region weld metal and limiting core region shell forging 05 (Heat no. 4853) exhibited shifts in RT_{NDT} of 80°F and 25°F, respectively. These shifts at a fluence of 2.20×10^{18} n/cm² are plotted in Figure A-1. A modified trend curve was developed for the weld metal by drawing a line parallel to the present trend curves through the surveillance data point. Figure A-1 shows the modified trend curve as a dashed line. The modified trend curve is used to obtain: the ΔRT_{NDT} in the weld metal, and the heatup and cooldown curves are based on this ΔRT_{NDT} . The resultant heatup and cooldown limit curves for normal operation of the reactor vessel are presented in Figures A-3 and A-4 and represent an operational time period of 9 effective full power years.

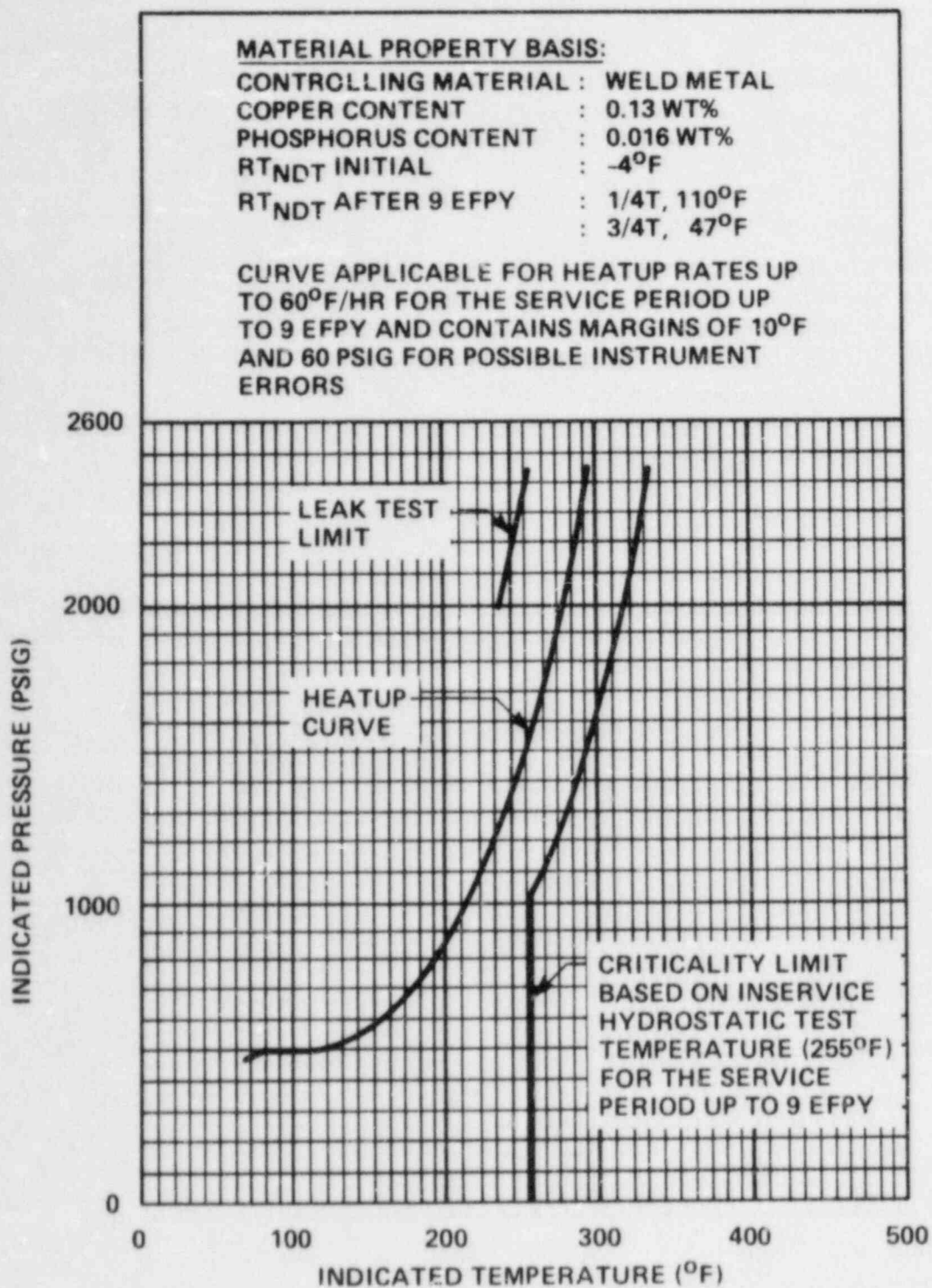


Figure A-3. Sequoyah Unit 2 Reactor Coolant System Heatup Limitations Applicable up to 9 EFY

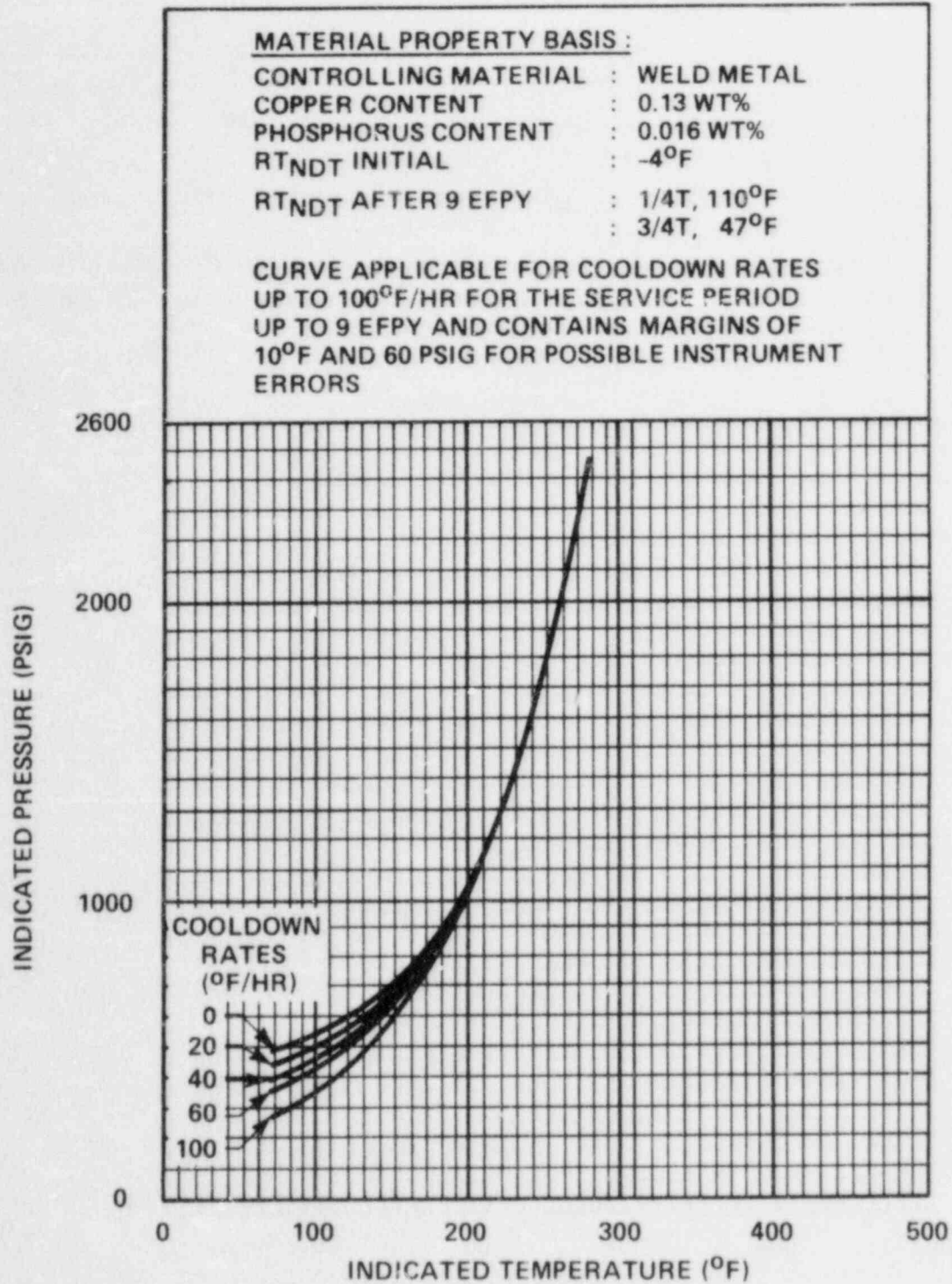


Figure A-4. Sequoyah Unit 2 Reactor Coolant System Cooldown Limitations
Applicable up to 9 EPFY

Allowable combinations of temperature and pressure for specific temperature change rates are below and to the right of the limit lines shown on the heatup and cooldown curves. The reactor must not be made critical until pressure-temperature combinations are to the right of the criticality limit line shown in Figure A-3. This is in addition to other criteria which must be met before the reactor is made critical.

The leak test limit curve shown in Figure A-3 represents minimum temperature requirements at the leak test pressure specified by applicable codes. The leak test limit curve was determined by methods of References 2 and 3.

Figures A-3 and A-4 define limits for insuring prevention of nonductile failure.

APPENDIX A REFERENCES

1. "Fracture Toughness Requirements," Branch Technical Position MTEB 5-2, Chapter 5.3.2 in Standard Review Plan for the Review of Safety Analysis Reports for Nuclear Power Plants, LWR Edition, NUREG-0800, 1981.
2. ASME Boiler and Pressure Vessel Code, Section III, Division 1 — Appendices, "Rules for Construction of Nuclear Vessels," Appendix G, "Protection Against Nonductile Failure," pp. 559-564, 1983 Edition, American Society of Mechanical Engineers, New York, 1983.
3. "Pressure-Temperature Limits," Chapter 5.3.2 in Standard Review Plan for the Review of Safety Analysis Reports for Nuclear Power Plants, LWR Edition, NUREG-0800, 1981.